Beam emittance measurement with laser wire scanners in the International Linear Collider beam delivery system

I. Agapov[*]

CERN, CH-1211 Geneva 23, Switzerland

G. A. Blair[†]

John Adams Institute at Royal Holloway University London, Egham, Surrey, TW20 0EX, United Kingdom

M. Woodley[‡]

SLAC, 2575 Sand Hill Road, Menlo Park, California 94025, USA
(Received 12 April 2007; published 9 November 2007)

Accurate measurement of the beam phase space is essential for the next generation of electron accelerators. A scheme for beam optics optimization and beam matrix reconstruction algorithms for the diagnostics section of the beam delivery system of the International Linear Collider (ILC) based on laser-wire beam profile monitors are discussed. Possible modes of operation of the laser-wire system together with their corresponding performance are presented. Based on these results, prospects for reconstructing the ILC beam emittance from representative laser-wire beam size measurements are evaluated.

PACS numbers: 41.75.Fr, 41.85.Qg

I. INTRODUCTION

Future electron machines will need accurate determination and monitoring of their transverse phase space in order to meet their challenging performance specifications. In this paper, prospects for the transverse emittance measurements at the International Linear Collider (ILC) are presented, with special emphasis on the beam delivery system (BDS).

The main parameters of the ILC [1,2] are presented in Table I.

The ILC luminosity L is given by [3]

$$L = \frac{N_{\text{train}} N_e^2 f}{4\pi \sigma_{ey}^* \sigma_{ex}^*} \times H_D, \tag{1}$$

where the asterisk denotes the value at the e^+e^- interaction point (IP). H_D is the disruption parameter due to the mutual attraction of electrons and positrons in the collision and has value $H_D \simeq 2$. Although the beam sizes at the IP depend strongly on the aberrations in the final-focus system, accurate measurement of beam parameters upstream of the final focus is required to tune the main linac performance. The information about the transverse beam phase space is gained by putting beam profile scanners at several locations along the beam line. The vertical beam sizes in the diagnostics section of the beam delivery system of the ILC are of order of 1 μm which is too small to measure with a solid wire, so the transverse beam profile measurements will be performed by the laser-wire (LW) system [4,5]. A

similar situation applies to portions of the ring-to-main-linac and the main linac sections of the ILC.

In contrast to a ring machine, where an individual bunch can be measured many times as it passes around the ring, the emittance measurement in the ILC BDS will need to be performed on a single-pass basis. This will require laser-wire scans that sample across successive bunches within a train, necessarily involving both a projection of any bunch position jitter and an averaging over successive bunches. The analysis described below of the extraction of the emittance from the bunch dimension measurements applies equally to circular and linear machines, although additional allowances for variations between ILC trains may also be necessary, for instance when performing quadrupole scans or measurements of linear dispersion. Throughout this paper, the electron bunch is assumed to be pure Gaussian; an extension of the analysis presented here to more realistic post-linac ILC bunch profiles will be included in a future publication.

In Sec. II the beam matrix reconstruction using a series of beam profile monitors is described. This section deals

TABLE I. Nominal ILC parameters.

Beam energy	E	250 (500)	GeV
Normalized horizontal emittance	$\gamma \epsilon_x$	10^{-5}	m rad
Normalized vertical emittance	$\gamma \epsilon_y$	4×10^{-8}	m rad
Train repetition rate	f	5	Hz
Number of bunches per train	N_{train}	2625	
Interbunch spacing		369	ns
Bunch length	L_b	300	μm
Number of electrons per bunch	N_e	2	$\times 10^{10}$

[*]Ilya.Agapov@cern.ch
[†]blair@pp.rhul.ac.uk
[‡]mwd@slac.stanford.edu

mostly with an analysis of how the emittance measurement error depends on the precision of the beam profile measurement. The general ideas behind the beam matrix reconstruction method described here are well known (see e.g. [6–9]). After presenting the framework we discuss numerical algorithms for matrix reconstruction and introduce a numerical criterion allowing beam optics optimization. Simulations of emittance reconstruction using ILC parameters are presented. The methods described in this section are independent of the type of the beam profile monitor or beam sizes.

In Sec. III the LW beam profile monitor is introduced and its use in the measurement of transverse beam profiles is described. The LW is useful as a noninvasive device to measure electron beam profiles ranging from a few tens of microns down to the micron scale. Issues of Gaussian beam optics that influence the measurement are discussed and quantitative results presented. We conclude by quoting the requirements on the laser-wire system, plus associated laser specifications necessary to achieve the desired emittance measurement precision of a few percent.

Laser-wire specifications are given for the beam sizes relevant to the 500 GeV beam (1 TeV center of mass) machine upgrade, which is more challenging because the bunches are smaller. Other issues such as beam matrix reconstruction methods are independent of the beam energy and the results shown are normally for the 250 GeV beam.

II. BEAM MATRIX RECONSTRUCTION

In this section we first describe the standard approach to reconstructing the 4D coupled beam matrix with the least-squares fit method [6]. In the presence of coupling the emittance reconstruction precision falls dramatically with the beam size measurement error. The Cholesky decomposition method is analyzed as an option to reduce this effect.

We further introduce a criterion which allows numerical optimization of beam line lattice parameters to minimize the error of the emittance measurement. The contributions to the beam profile scan from effects such as beam jitter is discussed towards the end of the section. The described methods were used to simulate the emittance reconstruction process with the ILC lattice and with the beam size measurement precision predicted in Sec. III.

A. Beam matrix reconstruction from measured beam sizes

One is generally interested in reconstructing the $(x, x', y, y', \frac{\Delta p}{p}, \Delta t)$ beam phase space. To the first order it is given by correlations like $\langle xx' \rangle$, $\langle x\frac{\Delta p}{p} \rangle$, etc. The transverse coordinates r can be represented as the sum of the betatron oscillations r_β and dispersive trajectory $\eta \frac{\Delta p}{p}$,

$$r = (x, x', y, y'), \qquad r_\beta = (x_\beta, x'_\beta, y_\beta, y'_\beta)$$

$$r = r_\beta + \eta \frac{\Delta p}{p},$$

where the dispersion vector is

$$\eta = (\eta_x, \eta'_x, \eta_y, \eta'_y).$$

Ideally dispersion should be zero in the diagnostics section. But in reality some residual dispersion can be present. The dispersion at the beginning of the transfer line is defined as [10]

$$\eta_0 = \left\langle r \frac{\Delta p}{p} \right\rangle \Big/ \delta_E^2,$$

where $\delta_E^2 = \langle (\frac{\Delta p}{p})^2 \rangle$ is the rms momentum spread. The transverse beam envelope matrix is then defined as

$$\sigma = \langle rr^T \rangle = \left\langle \left(r_\beta + \eta \frac{\Delta p}{p} \right) \left(r_\beta + \eta \frac{\Delta p}{p} \right)^T \right\rangle$$

or

$$\sigma = \begin{bmatrix} \langle x^2 \rangle & \langle xx' \rangle & \langle xy \rangle & \langle xy' \rangle \\ \langle xx' \rangle & \langle x'^2 \rangle & \langle x'y \rangle & \langle x'y' \rangle \\ \langle xy \rangle & \langle x'y \rangle & \langle y^2 \rangle & \langle yy' \rangle \\ \langle xy' \rangle & \langle x'y' \rangle & \langle yy' \rangle & \langle y'^2 \rangle \end{bmatrix}.$$

The equations for dispersion and betatron coordinates are [10]

$$r''_\beta + K(s)r_\beta = 0 \qquad \eta'' + K(s)\eta = \frac{1}{\rho},$$

where $1/\rho$ is the orbit curvature. We assume that in the diagnostics section the beam orbit is first aligned sufficiently close to the magnet axis so that the additional dispersion created there can be neglected. Then one can write down the coordinates at each scanner location i in terms of transfer matrices [11] as

$$r_{\beta,i} = R_i r_{\beta,0} \qquad \eta_i = R_i \eta_0$$

and thus

$$r_i = R_i \left(r_{\beta,0} + \eta_0 \frac{\Delta p}{p} \right) = R_i r_0 \qquad \sigma_i = R_i \sigma_0 R_i^T. \quad (2)$$

This definition of the beam matrix already includes effects of the dispersion.

The phase space occupied by a (generally coupled) beam can be quantified by the intrinsic emittances $\varepsilon_{1,2}$ [12]. They are recovered from the beam matrix constructed from the betatron coordinates only by bringing it to a diagonal form:

$$\sigma_\beta = \langle r_\beta r_\beta^T \rangle$$

$$\sigma_\beta = Q\bar{\sigma}_\beta Q^T \quad \bar{\sigma}_\beta = \begin{bmatrix} \varepsilon_1 & 0 & 0 & 0 \\ 0 & \varepsilon_1 & 0 & 0 \\ 0 & 0 & \varepsilon_2 & 0 \\ 0 & 0 & 0 & \varepsilon_2 \end{bmatrix}.$$

In what follows, "vertical" emittance usually denotes the smaller of the intrinsic emittances. The projected (vertical) emittance is defined as

$$\epsilon_y = \det \begin{bmatrix} \langle y^2 \rangle & \langle yy' \rangle \\ \langle yy' \rangle & \langle y'^2 \rangle \end{bmatrix}.$$

It will coincide with the intrinsic emittance if the beam is uncoupled but will be larger if the coupling is present. We can rewrite the beam matrix as

$$\sigma_0 = \begin{bmatrix} \sigma_1 & \sigma_2 & \sigma_3 & \sigma_4 \\ \sigma_2 & \sigma_5 & \sigma_6 & \sigma_7 \\ \sigma_3 & \sigma_6 & \sigma_8 & \sigma_9 \\ \sigma_4 & \sigma_7 & \sigma_9 & \sigma_{10} \end{bmatrix},$$

and we need at least ten measurements to accomplish the task. At a scanner location in the beam line it is possible to measure three values, $\langle x^2 \rangle$, $\langle y^2 \rangle$, and $\langle xy \rangle$, with the help of a horizontal, a vertical, and a tilted wire scanner. The ten values can be obtained either by changing the optics in a controlled manner at the wire location [6–8] or by locating the wires at different positions in the beam line. For the ILC, one aims at fast intratrain scanning for which the former method is not possible.

The elements of the beam matrix can be obtained analytically when the coupling elements are neglected and the total number of wire scanners is six (three for each plane, two scanners at each location) that are suitably spaced in the betatron phase [9]. For more general cases, it is however convenient to have a numerical procedure for the beam matrix reconstruction, which will be now described. Let the measured values of $\langle x^2 \rangle$, $\langle y^2 \rangle$, and $\langle xy \rangle$ be

$$\hat{\sigma}_1^i \quad \hat{\sigma}_8^i \quad \hat{\sigma}_3^i$$

with $i = 1:N_{\text{scanners}}$. Let σ_k be the elements of the beam matrix at the location where the beam transfer matrices R are evaluated from. Assuming that the transport matrices are uncoupled in the diagnostics section (coupling introduced by misalignment errors is neglected), one obtains by equating coefficients in Eq. (2)

$$\hat{\sigma}_1^i = R_{11,i}^2 \sigma_1 + 2R_{11,i}R_{12,i}\sigma_2 + R_{12,i}^2 \sigma_5$$
$$\hat{\sigma}_8^i = R_{33,i}^2 \sigma_8 + 2R_{33,i}R_{34,i}\sigma_9 + R_{34,i}^2 \sigma_{10}$$
$$\hat{\sigma}_3^i = R_{11,i}R_{33,i}\sigma_3 + R_{11,i}R_{34,i}\sigma_4 + R_{12,i}R_{33,i}\sigma_6$$
$$+ R_{12,i}R_{34,i}\sigma_7$$

for $i = 1:N_{\text{scanners}}$. Define:

$$M_X = \begin{bmatrix} R_{11,1}^2 & 2R_{11,1}R_{12,1} & R_{12,1}^2 \\ R_{11,2}^2 & 2R_{11,2}R_{12,2} & R_{12,2}^2 \\ R_{11,3}^2 & 2R_{11,3}R_{12,3} & R_{12,3}^2 \\ \cdots & \cdots & \cdots \end{bmatrix}$$

$$M_Y = \begin{bmatrix} R_{33,1}^2 & 2R_{33,1}R_{34,1} & R_{34,1}^2 \\ R_{33,2}^2 & 2R_{33,2}R_{34,2} & R_{34,2}^2 \\ R_{33,3}^2 & 2R_{33,3}R_{34,3} & R_{34,3}^2 \\ \cdots & \cdots & \cdots \end{bmatrix}$$

$$M_{XY} = \begin{bmatrix} R_{11,1}R_{33,1} & R_{11,1}R_{34,1} & R_{12,1}R_{33,1} & R_{12,1}R_{34,1} \\ R_{11,2}R_{33,2} & R_{11,2}R_{34,2} & R_{12,2}R_{33,2} & R_{12,1}R_{34,2} \\ R_{11,3}R_{33,3} & R_{11,3}R_{34,3} & R_{12,3}R_{33,3} & R_{12,1}R_{34,3} \\ \cdots & \cdots & \cdots & \cdots \end{bmatrix}.$$

The problem then reduces to three uncoupled sets of equations:

$$M_X \begin{bmatrix} \sigma_1 \\ \sigma_2 \\ \sigma_5 \end{bmatrix} = \begin{bmatrix} \hat{\sigma}_1^1 \\ \hat{\sigma}_1^2 \\ \cdots \end{bmatrix}, \qquad M_Y \begin{bmatrix} \sigma_8 \\ \sigma_9 \\ \sigma_{10} \end{bmatrix} = \begin{bmatrix} \hat{\sigma}_8^1 \\ \hat{\sigma}_8^2 \\ \cdots \end{bmatrix},$$

$$M_{XY} \begin{bmatrix} \sigma_3 \\ \sigma_4 \\ \sigma_6 \\ \sigma_7 \end{bmatrix} = \begin{bmatrix} \hat{\sigma}_3^1 \\ \hat{\sigma}_3^2 \\ \cdots \end{bmatrix} \tag{3}$$

and each set is solved separately by a least-squares fit. This may lead to an unphysical result (a nonpositive beam matrix) when the measurement is sufficiently noisy. A typical dependency of the fraction of nonpositive matrices on the relative measurement error is shown in Fig. 1. Here the 4D diagnostics section with 6 laser-wire stations and nominal ILC parameters were assumed. A common relative measurement error is assumed for both the horizontal
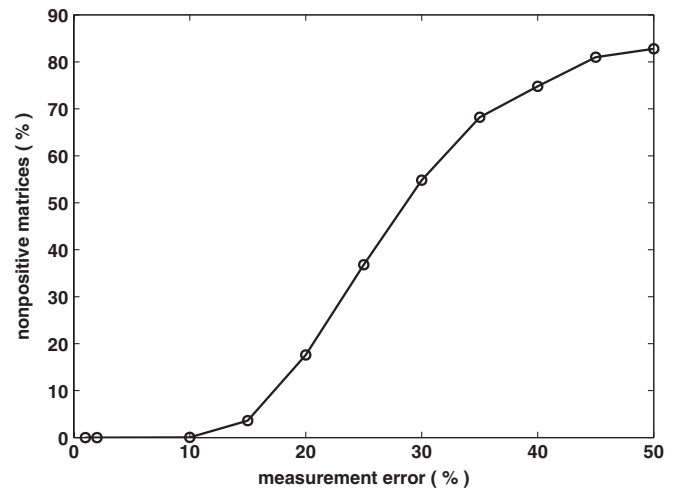

FIG. 1. Beam matrix rejection fraction vs relative beam size measurement error level for the 4D ILC emittance measurement section with 6 scanners.

and vertical dimensions, for reasons outlined below in Sec. II C 4.

A way to avoid nonpositive beam matrices is to search for the beam matrix as a Cholesky decomposition [13,14]

$$\sigma_0 = GG^T$$

where $G \in \mathbb{R}^{4 \times 4}$ is lower (or upper) triangular with positive diagonal entries. From the point of view of numerical errors, the lower triangular representation should be used when the horizontal emittance is smaller than the vertical, and the upper in the opposite case. This procedure introduces biasing to the emittance measurement, however it seems to be advantageous when either a small number of measurements is available or when a larger measurement error results in a high rejection fraction (fraction of nonpositive matrices). In Figs. 2 and 3 examples of emittance fits using simulated beam size measurement data in the 4D ILC emittance measurement section are shown. A relative error of 35% was introduced to the simulated data. Both methods yield a significantly biased mean emittance. However, the Cholesky decomposition method results in an increase of statistics (i.e. physically meaningful fits) by a factor of 3.

When large statistics are available, the straightforward method performs satisfactorily. For the ILC one aims at about 1%–5% measurement errors within a bunch train. In this range the choice of algorithm is not important during stable operation, however the Cholesky decomposition method will be helpful in certain cases, for instance during the measurement tune-up when the errors are large.

In the presence of coupling, the intrinsic emittance is smaller than the projected one. With measurement errors the center of the distribution of reconstructed intrinsic emittances is shifted towards smaller values even if the real beam is uncoupled [12] (also seen in Figs. 2 and 3).
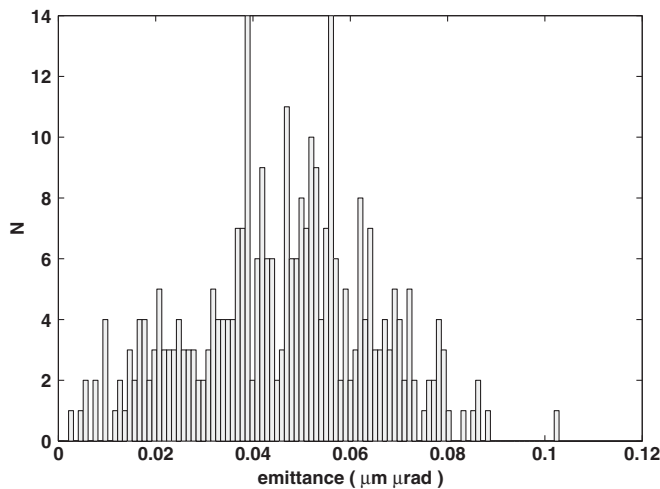

FIG. 2. Example of a direct least-squares emittance fit (35% error level, 4D ILC optics). The true emittance is 0.079 μm $\cdot$ μrad.
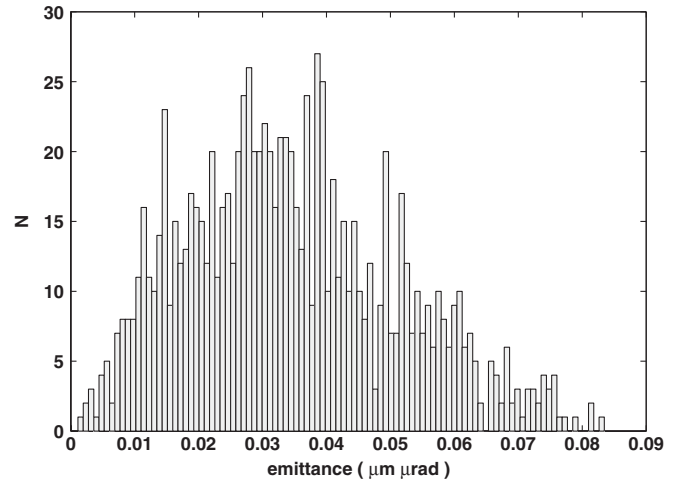

FIG. 3. Example of a least-squares emittance fit with the Cholesky decomposition (35% error level, 4D ILC optics). The amount of statistics with the Cholesky method is about 3 times larger. It is however more biased. The true emittance is 0.079 μm $\cdot$ μrad.

The distribution of projected emittances does not shift, so care should be taken if the difference between the projected and the intrinsic emittances is used to evaluate the coupling correction.

When beam position measurements are available and it is possible to vary the beam energy, the dispersion functions can be measured at wire locations. Supposing the measurement vector is $\{\hat{\eta}_i\}$, the initial dispersion is recovered with a least-squares fit from

$$M_{\eta X, \eta Y} \begin{bmatrix} \eta_{X0,Y0} \\ \eta'_{X0,Y0} \end{bmatrix} = \hat{\eta}^i_{X,Y}$$

with

$$M_{\eta X} = \begin{bmatrix} R_{11,1} & R_{12,1} \\ R_{11,2} & R_{12,3} \\ R_{11,3} & R_{12,4} \\ \cdots & \cdots \end{bmatrix} \qquad M_{\eta Y} = \begin{bmatrix} R_{33,1} & R_{34,1} \\ R_{33,2} & R_{34,3} \\ R_{33,3} & R_{34,4} \\ \cdots & \cdots \end{bmatrix}.$$

The dispersion model used here might not be adequate since in reality the bunches coming from the linac might have a complicated correlation pattern. Its correction in combination with the emittance measurement is the subject of a separate work. So in what follows we will not analyze the effect of dispersion apart from estimating its influence on the beam profile measurement.

B. Beam optics for the diagnostics section

Concepts of optics for 2D and 4D diagnostics sections were presented in [15]. For optimal performance the diagnostics section lattice should be designed so that the beam sizes and aspect ratios at the wire location are optimal for scanning performance and that the solutions of Eqs. (3) are only weakly sensitive to perturbations of the right-hand

side. For optics analysis it is convenient to express the R-matrices in terms of Twiss parameters [16]. In the uncoupled case

$$R = \begin{bmatrix} R_{(x)} & 0 \\ 0 & R_{(y)} \end{bmatrix},$$

where, assuming periodic optics,

$$M_X = \begin{bmatrix} \cos^2\Delta\mu_{x,1} & 2\beta_x\cos\Delta\mu_{x,1}\sin\Delta\mu_{x,1} & \beta_x^2\sin^2\Delta\mu_{x,1} \\ \cos^2\Delta\mu_{x,2} & 2\beta_x\cos\Delta\mu_{x,2}\sin\Delta\mu_{x,2} & \beta_x^2\sin^2\Delta\mu_{x,2} \\ \cos^2\Delta\mu_{x,3} & 2\beta_x\cos\Delta\mu_{x,3}\sin\Delta\mu_{x,3} & \beta_x^2\sin^2\Delta\mu_{x,3} \\ \cdots & \cdots & \cdots \end{bmatrix}$$

$$M_Y = \begin{bmatrix} \cos^2\Delta\mu_{y,1} & 2\beta_y\cos\Delta\mu_{y,1}\sin\Delta\mu_{y,1} & \beta_y^2\sin^2\Delta\mu_{y,1} \\ \cos^2\Delta\mu_{y,2} & 2\beta_y\cos\Delta\mu_{y,2}\sin\Delta\mu_{y,2} & \beta_y^2\sin^2\Delta\mu_{y,2} \\ \cos^2\Delta\mu_{y,3} & 2\beta_y\cos\Delta\mu_{y,3}\sin\Delta\mu_{y,3} & \beta_y^2\sin^2\Delta\mu_{y,3} \\ \cdots & \cdots & \cdots \end{bmatrix}$$

and

$$M_{XY} = \{m_{XY}^{ij}\} \qquad (4)$$

$$m_{XY}^{i,1} = \frac{1}{2}[\cos(\Delta\mu_x - \Delta\mu_y) + \cos(\Delta\mu_x + \Delta\mu_y)]$$

$$m_{XY}^{i,2} = \frac{\beta_y}{2}[\sin(\Delta\mu_x + \Delta\mu_y) - \sin(\Delta\mu_x - \Delta\mu_y)]$$

$$m_{XY}^{i,3} = \frac{\beta_y}{2}[\sin(\Delta\mu_x + \Delta\mu_y) + \sin(\Delta\mu_x - \Delta\mu_y)]$$

$$m_{XY}^{i,4} = \frac{\beta_x\beta_y}{2}[\cos(\Delta\mu_x - \Delta\mu_y) - \cos(\Delta\mu_x + \Delta\mu_y)]..$$

$$(5)$$

One can choose the optimality criterion for the lattice to be the condition numbers of the corresponding matrices [13,14],

$$\kappa_i = \text{cond}(M_i) = \|M_i\|\|M_i^{-1}\|.$$

Here the norm of a matrix M is defined as the maximum value of $\|Mx\|$ over all vectors of unit lengths

$$\|M\| = \max_{\|x\|=1}\|Mx\|.$$

The condition number is used to quantify the solution error of a linear algebraic system [13,14]. A small condition number corresponds to well-conditioned systems while a large condition number corresponds to ill-conditioned systems. This number is hard to evaluate analytically but it can be evaluated numerically for any optics design. Apart from the condition number, one has to make sure that both x and x' make contributions of the same order of magnitude to the measurements, i.e., (for the 2D case),

$$R_{(x,y)} = \begin{bmatrix} \cos\Delta\mu + \alpha\sin\Delta\mu & \beta\sin\Delta\mu \\ -\frac{(1+\alpha^2)}{\beta}\sin\Delta\mu & \cos\Delta\mu - \alpha\sin\Delta\mu \end{bmatrix}.$$

Assuming further that the wire locations are at the maxima of the β-functions in order to optimize the spot-size resolution, α vanishes and the matrices M_X, M_Y, and M_{XY} will have the form

$$R_{11}x \approx R_{12}x'$$

or

$$\beta\tan(\mu)\frac{x'}{x} \approx 1.$$

To achieve this, one can introduce another optimality criterion to minimize:

$$\left|\beta\tan(\mu)\frac{x'}{x}\right| + \frac{1}{|\beta\tan(\mu)\frac{x'}{x}|} \rightarrow \min. \qquad (6)$$

For the full beam matrix reconstruction, one needs to have ten measurements including coupling terms. Beam optics for such a measurement section should be designed so that the condition numbers of M_X, M_Y, and M_{XY} are minimized simultaneously (so-called 4D optics). In many cases, one is interested only in correcting the coupling terms rather than measuring them. To do so, a set of skew quadrupoles is introduced upstream of the measurement section. They are used to minimize the projected emittances [12] and no direct measurement of the coupling terms is necessary. In this case six measurements are required and the condition numbers of only M_X and M_Y need to be minimized (so-called 2D optics).

1. 2D measurement section

For the diagnostic section lattice we choose a FODO channel with a constant phase advance per cell $\Delta\mu_1 = \Delta\mu_2 = \Delta\mu$. Then κ will depend on two parameters: β and $\Delta\mu$. In Fig. 4 and 5 these dependencies are shown for different numbers of measurement stations.

The condition number is infinite for 0° and 90° phase advance (not seen in the picture). It has a minimum close to 0° and a second minimum that depends on the number of
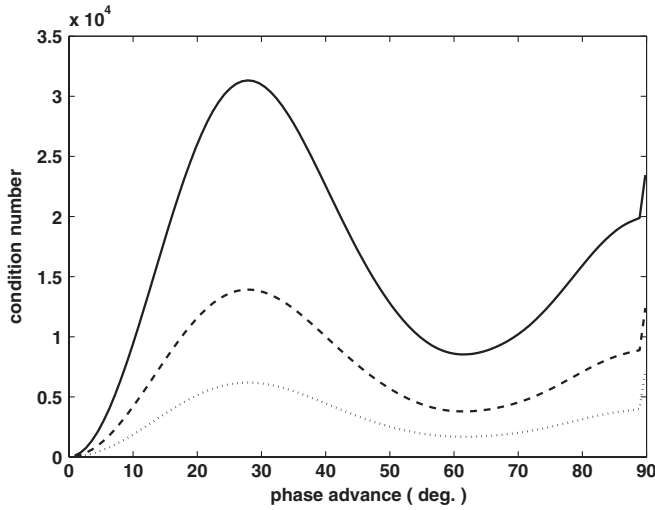
FIG. 4. Condition number of M_X (or M_Y) plotted against cell phase advance for β-function 90 m (solid line), 60 m (dashed line), and 40 m (dotted line). 3 wire scanners.

wire scanners used in the fit. This minimum appears to be at $\Delta\mu = 180°/N_{scanners}$ (60° for 3 scanners). Together with Eq. (6) (see also Fig. 6), this gives $180°/N_{scanners}$ as the optimal phase advance in a FODO cell. In Fig. 7 simulated emittance reconstruction error is plotted against the cell phase advance which shows that the error is indeed minimized by following the described optimization procedure.

2. 4D measurement section

For a 4D diagnostics section we can assume that the lattice is constructed from identical cells of phase advances $\Delta\mu_1$ and $\Delta\mu_2$. The matrix M depends on 4 parameters $\beta_{1,2}$ and $\Delta\mu_{1,2}$. For different values of $\beta_{x,y}$ the behavior shows
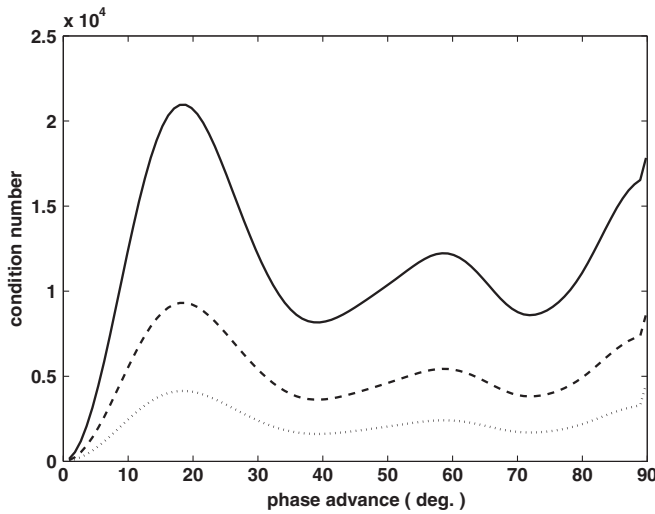

FIG. 5. Condition number of M_X (or M_Y) plotted against cell phase advance for β-function 90 m (solid line), 60 m (dashed line), and 40 m (dotted line). 5 wire scanners.
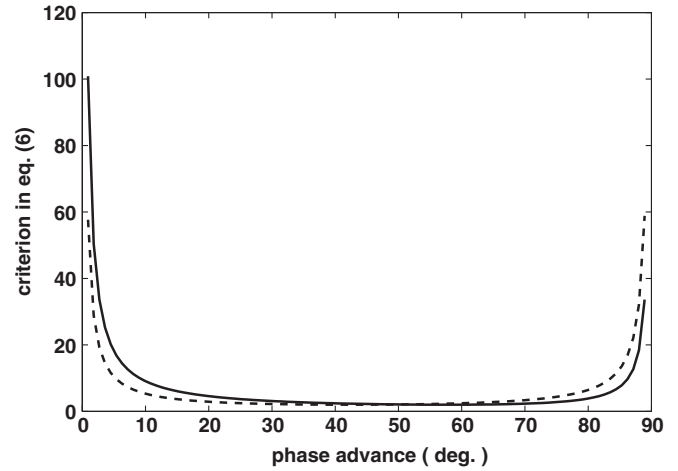

FIG. 6. Value of (6) plotted against cell phase advance for β-function 40 m (solid line) and 70 m (dashed line).

a similar pattern with the matrix being singular for $\Delta\mu_1 = \Delta\mu_2$ and $\Delta\mu_1 = 180° - \Delta\mu_2$. Combining the information on plots such as in Fig. 8 with that in Figs. 4 and 5, one sees that there is no clear optimum for this problem. However, for a good performance one can choose, for instance, a phase advance in one plane of 60° and in the other plane a phase advance close to 90° (for 4 wire stations with 3 wires each).

The optics for the ILC diagnostics sections [15] designed for 2D and 4D emittance measurements are shown in Fig. 9. The 2D diagnostics section is sufficient for emittance tuning purposes and is shorter; it is thus currently expected to be used at the ILC [1,2].

C. Machine contributions to the transverse profile scans

The imperfections in the linac will result in beam jitter, residual dispersion, transverse beam coupling, etc. [17,18].
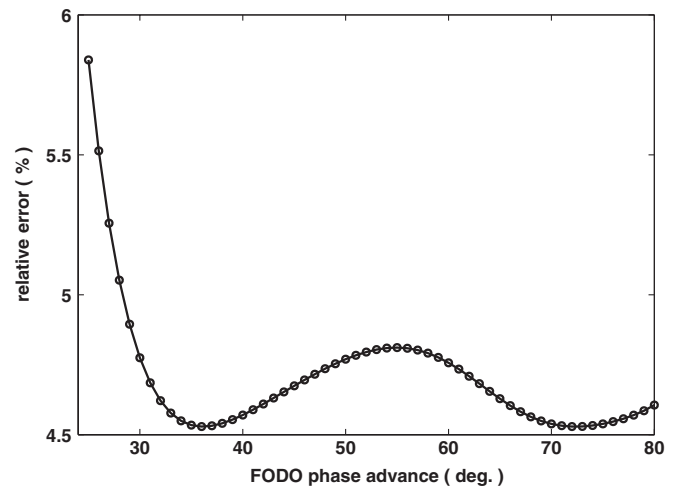

FIG. 7. Simulated vertical emittance reconstruction error vs cell phase advance, 5 wire scanners, 5% error on beam size measurement.
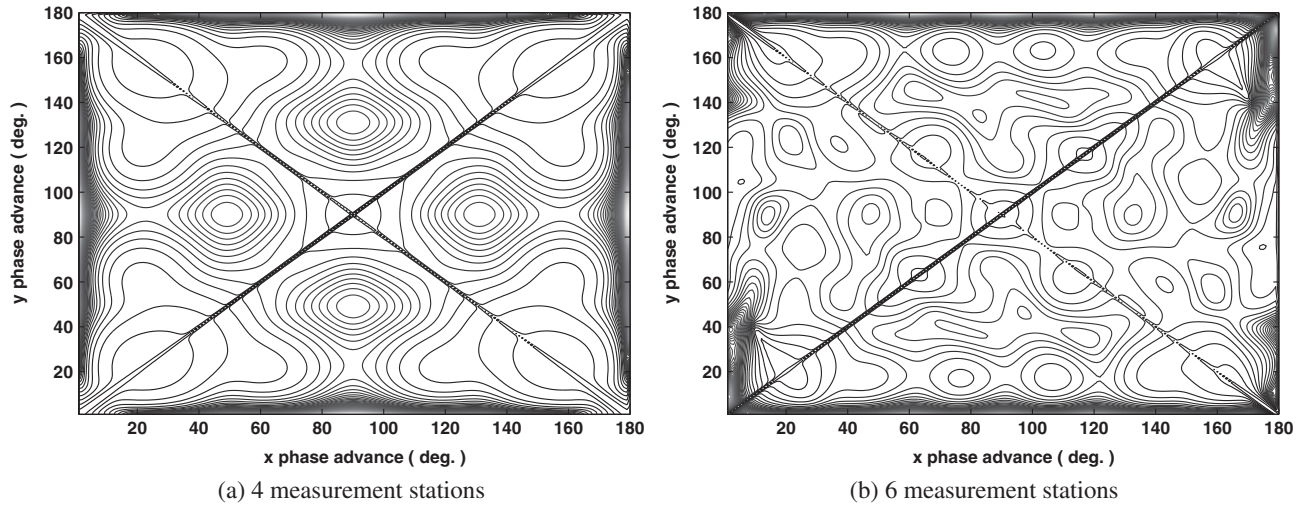
(a) 4 measurement stations

(b) 6 measurement stations

FIG. 8.   Contour plots of $2/(1 + \kappa_{XY})$ for M_{XY} as a function of cell phase advances for 4 wire stations and 6 wire stations with $\beta_{x,y} = 40$ m/70 m.
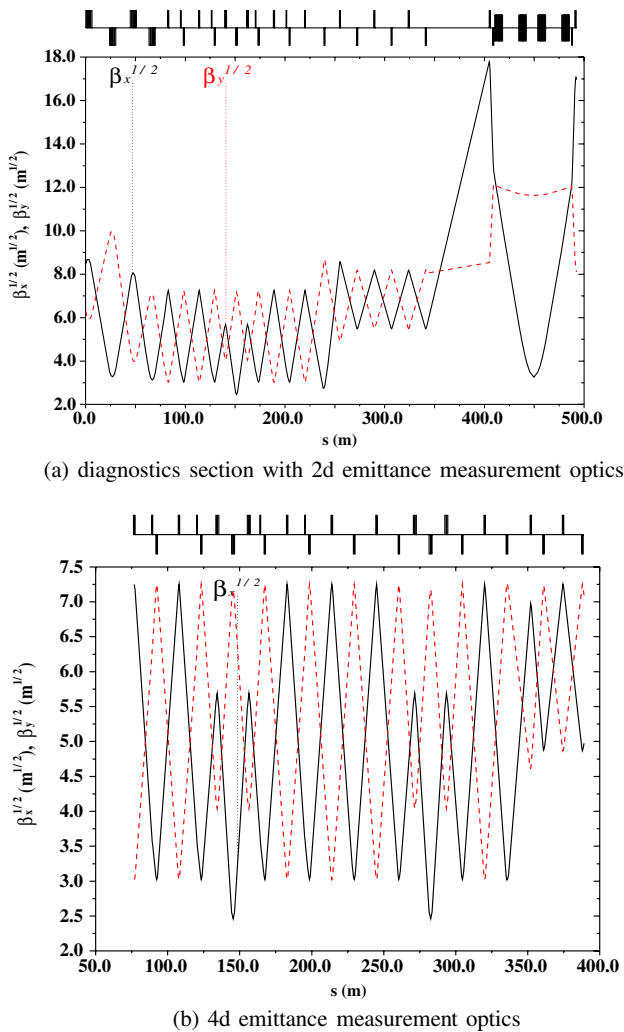

(a) diagnostics section with 2d emittance measurement optics

(b) 4d emittance measurement optics

FIG. 9. (Color) β-functions for the ILC diagnostics section comprising a 2D emittance measurement section; β-functions for the 4D emittance measurement section.

These may also cause a deviation of the bunch from the Gaussian shape. Estimates of these errors can partially be subtracted from the beam size measurements. Because of imperfections in the diagnostic section, the transfer matrices will also not be known precisely, which will introduce additional errors into the reconstruction procedure; this effect is expected to be much smaller than the others and is neglected in this paper.

Neglecting all but the dispersion and beam jitter contributions, the value of σ_e extracted from the beam profile scan is

$$\sigma_e = [\sigma_{\text{scan}}^2 - (\alpha_J \sigma_e)^2 - (\eta \delta_E)^2]^{1/2}, \qquad (7)$$

where σ_{scan} is the laser-wire scan after deconvolution of laser effects (discussed in Sec. III A 4) and α_J represents the magnitude of the beam orbit jitter, as normalized by the observed beam size, and will be detailed in the next section.

When an effect contributes to the measurement error $\delta\sigma_e/\sigma_e$, we define E_{effect} as its contribution to the total relative error, adding in quadrature as

$$\left(\frac{\delta\sigma_e}{\sigma_e}\right)^2 = E_{\text{scan}}^2 + E_{\text{jitter}}^2 + E_\eta^2, \qquad (8)$$

where E_{scan} is the contribution to the error from the raw laser-wire scan; the contributions to this error are discussed in Sec. III A 4. E_{jitter} is the error remaining after subtracting the electron bunch-to-bunch jitter as discussed in Sec. II C 1. The additional effects of any residual dispersion, E_η, could in principle also be subtracted explicitly; the error that remains after such a subtraction is estimated below.

The significant machine-related errors are now discussed in turn.

I. AGAPOV, G. A. BLAIR, AND M. WOODLEY

Phys. Rev. ST Accel. Beams **10,** 112801 (2007)

1. Error contribution from the jitter of the beam location

In the following, the jitter of the location of the bunches within the bunch train at the ILC laser-wire IP locations can be written as $\sigma_{\text{jitter}} = \alpha_J \sigma_e$ where σ_e is the electron transverse bunch size. The value of α_J will depend on the stability of the ILC site and on the additional vibrations arising from beam line components, from energy and kicker jitter, and from the performance of train-to-train and intratrain feedback. Preliminary studies [19] suggest that values of α_J may end up ranging from about 0.01 to about 0.7; in the following the resulting error estimates are normalized relative to a value $\alpha_J \simeq 0.25$. The bunch-by-bunch jitter can be determined by local BPMs to within their single-bunch resolution. The performance of cavity BPMs is the subject of ongoing research and development (R&D) [20], which suggests that single-bunch resolutions of order 20 nm should be obtainable.

The error contribution E_{jitter} to $\delta\sigma_e/\sigma_e$ remaining after subtracting the bunch jitter is given by differentiating Eq. (7) to be

$$E_{\text{jitter}} = \alpha_J \langle \delta\alpha_J \rangle \simeq \alpha_J \frac{\sigma_{\text{BPM}}}{\sigma_e},$$

where $\langle \delta\alpha_J \rangle$ is the precision to which the bunch jitter is known; the last approximation assumes that the only bunch jitter measurements are made at the LW location. It is possible that more precise measurements could be made using dedicated machine setups. This equation can be written as

$$E_{\text{jitter}} = 5 \times 10^{-3} \left(\frac{\alpha_J}{0.25} \right) \left(\frac{\sigma_{\text{BPM}}}{20 \text{ nm}} \right) \left(\frac{1 \ \mu\text{m}}{\sigma_e} \right). \quad (9)$$

2. Error contribution from residual dispersion

If the effects of η and η' are not subtracted at the location of each LW IP, then the emittance will be overestimated. The error remaining after subtraction of residual vertical dispersion, η, at the laser-wire IP is again given by differentiation of Eq. (7) to be

$$E_\eta = \left(\frac{\delta_E}{\sigma_{ey}} \right)^2 \eta \langle \delta\eta \rangle, \quad (10)$$

where $\langle \delta\eta \rangle$ is the precision to which η can be determined. If E_η is not to dominate a 1% transverse bunch size measurement for a typical ILC beam then E_η should be less than about 0.5%. If η is measured to $\langle \delta\eta \rangle/\eta \simeq 1\%$, say, then for $\sigma_{ey} = 1 \ \mu$m Eq. (10) implies that η must be kept below about 0.5 mm.

A method that could potentially be used to determine η more accurately than 1% is to change the mean energy of the electron beam by a relative amount $\Delta E/E$ (a possible choice would be $\Delta E/E \simeq 5 \times 10^{-3}$ so as to remain within the energy acceptance of the ILC BDS) and measure any subsequent shift in position of the beam centroid over the

N_{train} bunches in a train. If the single-bunch energy resolution of the ILC beam spectrometers is σ_E, then

$$\langle \delta\eta \rangle^2 = \frac{1}{N_{\text{train}}} \left[\frac{(\eta\sigma_E)^2 + \sigma_{\text{BPM}}^2}{(\Delta E/E)^2} \right]. \quad (11)$$

With additional R&D, it should be possible to achieve $\sigma_{\text{BPM}} \simeq 20$ nm and spectrometer resolution $\sigma_E \simeq 10^{-4}$ [21]. An alternative to explicit subtraction of the dispersion effects is to include them implicitly in the fits to the measured laser-wire distribution; this is the method described above in Sec. II A.

3. Systematic beam size variations

In general, position shifts of individual bunches within a linear collider bunch train can have arbitrary patterns according to the errors of the injection kickers, or effects of the long-range transverse wakefield. Regardless of the shape of the patterns, the individual relative bunch displacements can be subtracted using bunch-by-bunch BPM measurements and so such effects can be absorbed into the treatment of beam position jitter discussed in Sec. II C 1. Ideally the laser-wire fast scanning system will be able to take account of these patterns (for instance by learning the shape from previous trains) so as to maintain an efficient scanning technique across the length of a train.

One possible use of the laser-wire measurements will be to predict the spot size at the IP and thereby enable a comparison with the spot size inferred from luminosity measurements via Eq. (7). Systematic variations of the bunch transverse dimension along the train will lead to a bias in such predictions. For example, a distortion of the transverse dimension with maximum value $\pm s_{\text{train}}\sigma_e$, which varies linearly along the train, will modify the effective transverse dimension that enters Eq. (1) by

$$\left\langle \frac{1}{\sigma_e} \right\rangle \simeq \frac{1}{\bar{\sigma}_e} \left(1 + \frac{1}{3} s_{\text{train}}^2 \right). \quad (12)$$

In order to correct for such effects, a number of scans will need to be made within a train, requiring ultrafast scanning methods. Ongoing R&D [22] is aiming at scanning rates of several tens of kHz using electro-optic techniques.

The influence of the beam jitter on the measurement procedure depends strongly on the linac tuning procedure and requires further studies.

4. Vertical-horizontal coupling

One can measure $\langle x^2 \rangle = \sigma_x^2$, $\langle y^2 \rangle = \sigma_y^2$ and extract $\langle xy \rangle$ from an additional measurement of the bunch along the u-axis $\langle u^2 \rangle = \sigma_u^2$, which is defined to be at an angle ϕ with respect to the x-axis, as shown in Fig. 10:

$$\sigma_u^2 = \sigma_x^2 \cos^2\phi + \sigma_y^2 \sin^2\phi + 2\langle xy \rangle \cos\phi \sin\phi. \quad (13)$$
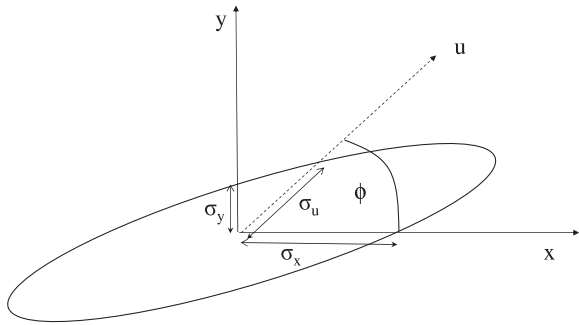
FIG. 10.   Bunch with horizontal-vertical coupling, such that its major axis does not lie along the horizontal. In addition to vertical and horizontal scans, a scan of the u-axis is necessary, where u is at an angle ϕ to the vertical as shown.

When it comes to measurement of σ_u with a LW, it will be necessary to take into account the size of the perpendicular dimension, because of Rayleigh-range effects discussed below.

The coupling $\langle xy \rangle$ is

$$\langle xy \rangle = \frac{\sigma_u^2}{2\cos\phi\sin\phi} - \frac{\sigma_x^2\cos\phi}{2\sin\phi} - \frac{\sigma_y^2\sin\phi}{2\cos\phi}. \quad (14)$$

The rms error $\delta\langle xy \rangle$ on the measurement of the coupling term is then given by

$$(\delta\langle xy \rangle)^2 = \left(\frac{\sigma_u^2}{\cos\phi\sin\phi}\frac{\delta\sigma_u}{\sigma_u}\right)^2 + \left(\frac{\sigma_x^2\cos\phi}{\sin\phi}\frac{\delta\sigma_x}{\sigma_x}\right)^2$$
$$+ \left(\frac{\sigma_y^2\sin\phi}{\cos\phi}\frac{\delta\sigma_y}{\sigma_y}\right)^2. \quad (15)$$

By substituting Eq. (13) into Eq. (15) and minimizing with respect to ϕ under the assumption that the relative errors $\delta\sigma_y/\sigma_y$ and $\delta\sigma_x/\sigma_x$ are approximately equal, the optimal value for ϕ is given by

$$\phi_0 = \tan^{-1}\left(\frac{\sigma_x}{\sigma_y}\right). \quad (16)$$

Substituting this value of ϕ into Eq. (15) and using the approximation that $\langle xy \rangle$ is small gives the error on the coupling term as

$$\delta\langle xy \rangle = \sigma_y\sigma_x\left[4\left(\frac{\delta\sigma_u}{\sigma_u}\right)^2 + \left(\frac{\delta\sigma_x}{\sigma_x}\right)^2 + \left(\frac{\delta\sigma_y}{\sigma_y}\right)^2\right]^{1/2}. \quad (17)$$

Typical values of interest to the ILC BDS are presented below in Table II, where it can be seen that for the optimal value of ϕ, $\sigma_u \approx \sigma_y$. With this optimal u-wire angle, the relative errors of the vertical and horizontal measurements enter equally in the coupling term in Eq. (17). This justifies the earlier simplification (Sec. II A), where equal relative errors were assumed for all measurements in the emittance reconstruction simulations. Also, since $\sigma_x > \sigma_y$ for the ILC, the error on the coupling given by Eq. (17) will grow more rapidly than the error on the vertical beam size as the relative measurement errors increase. This explains the fact that the number of unphysical beam matrices grows rapidly with the measurement error, because the coupling terms quickly dominate over those of the vertical part of the beam matrix.

III. THE LASER-WIRE IN BEAM EMITTANCE MEASUREMENT

In this section the laser-wire (LW) beam profile monitor is described and the possible precisions that can be obtained from its use in transverse beam profile measurements are quantified. Ideally the LW will be used at the ILC to measure the electron transverse beam profile at several locations within a bunch train (containing 2625 bunches, Table I), which will require high-power lasers to get sufficient statistics for each laser shot together with ultrafast laser scanning systems.

The LW is useful for beam profiles ranging from several tens of microns, down to the micron scale. Smaller beam profiles have been measured using laser interferometric techniques [5,23] whereas traditional solid wires or screens can be used for larger profiles (although they are disruptive to the electron beams). Very challenging, low f-number, laser optics are necessary for the LW in order to achieve the required small laser spot sizes and the subsequent performance is evaluated numerically and described in Sec. III A 3. The laser systems necessary to power the LW are also very challenging and the necessary specifications are derived and discussed in Sec. III D 1.

TABLE II.   The relevant measurables for emittance measurement under the approximation $\sigma_{xy} \simeq 0$ for a set of electron beam sizes of interest at the ILC for the given beam energies E_b. The quoted precisions for $\frac{\delta\langle xy \rangle}{\langle xy \rangle}$ are those obtainable if each of the dimensions σ_x, σ_y, and σ_u can be measured to 1%. The corresponding precisions for $\frac{\delta\sigma_x^2}{\sigma_x^2}$ and $\frac{\delta\sigma_y^2}{\sigma_y^2}$ are then both 2%.

| E_b | σ_x | σ_y | ϕ | σ_u | σ_v | Precision (μm)^2 | | |
GeV	μm	μm	deg	μm	μm	$\delta(\sigma_x^2)$	$\delta(\sigma_y^2)$	$\delta\langle xy \rangle$
500	9	1.4	81.2	1.95	8.89	1.62	0.04	0.30
500	15	1.4	84.7	1.97	14.9	4.5	0.039	0.51
250	14	2	81.8	2.8	13.8	3.92	0.08	0.68
250	20	1.8	84.8	2.53	19.9	8.0	0.06	0.88

I. AGAPOV, G. A. BLAIR, AND M. WOODLEY

Phys. Rev. ST Accel. Beams **10**, 112801 (2007)

A. The laser-wire beam profile monitor

Traditionally the transverse dimensions of an electron beam have been measured by scanning a tungsten or carbon wire across the beam and measuring the resulting backgrounds as a function of relative position of the wire. This method has the disadvantage of being highly disruptive to the electron beam and so it cannot be used during normal luminosity running. At the ILC, the electron beams in the BDS will have vertical transverse size of order 1-few μm; a normal wire scanner would not be able to measure beams of this size, nor would it be able to withstand the energy depositions from such high intensities.

To solve these issues, the solid wire can be replaced by a finely focused beam of laser light; such a system is called a laser-wire (LW). The Compton collisions between laser photons and beam electrons are detected downstream and the Compton rate as a function of relative positions of electron and laser beams provides the measurement of the electron beam transverse profile. This principle is illustrated in Fig. 11. Two distinct methods have been employed to date. Operating the laser in continuous wave mode together with a Fabry-Perot cavity to enhance the power has been used [24] at the accelerator test facility (ATF) at the KEK laboratory to measure the emittance of the damping ring; this technique would also be applicable to the ILC damping rings. In other parts of the machine, including the BDS, the beam is not circulating so a single-pass method based on high-power pulsed lasers is required [25–27]. In the following discussion, the latter technique is assumed.

1. Laser-wire Compton rates

The Compton cross section decreases as the electron beam energy increases. For an electron beam energy E_b
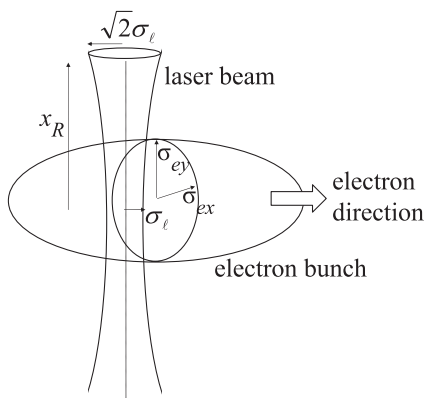

FIG. 11. Principle of operation of the laser-wire scanner with the key dimensions labeled. The figure shows the laser configured to scan the horizontal x-profile of the electron bunch σ_{ex}. x_R is the "Rayleigh range" of the laser beam as defined in Eq. (24); it gives the distance between the focus and the point where the laser-spot size has diverged to $\sqrt{2}$ of its minimum value.

TABLE III. Values of $f(\omega)$ for various laser wavelengths λ and ILC beam energies.

E_b (GeV)	λ (nm)			
	1064	532	355	266
5	0.96	0.92	0.89	0.86
50	0.72	0.59	0.51	0.45
150	0.51	0.38	0.31	0.27
250	0.41	0.30	0.24	0.20
500	0.30	0.20	0.16	0.13

and laser photon energy $k = \frac{hc}{\lambda}$, the Compton cross section is given by $\sigma_C(\omega) = \sigma_T f(\omega)$, where σ_T is the Thomson cross section $= 0.665 \times 10^{-28}$ m^2, $\omega = \frac{kE_b}{m_e^2}$, and [5,28]

$$f(\omega) = \frac{3}{4} \left\{ \frac{1+\omega}{\omega^3} \left[\frac{2\omega(1+\omega)}{1+2\omega} - \ln(1+2\omega) \right] \right.$$
$$\left. + \frac{\ln(1+2\omega)}{2\omega} - \frac{1+3\omega}{(1+2\omega)^2} \right\}.$$

Values of $f(\omega)$ for laser wavelengths and beam energies of typical interest at the ILC are presented in Table III.

In this section, the Compton rate for a set of laser-wire operating conditions is derived as a function of relative horizontal and vertical offsets, Δ_x and Δ_y, respectively, between the centroids of the electron bunch and laser beam.

The number $N(\Delta_x, \Delta_y)$ of Compton photons produced will be proportional to the relevant overlap integral, $\epsilon(\Delta_x, \Delta_y)$. In Appendix A 1, $\epsilon(\Delta_x, \Delta_y)$ will be evaluated in μm^{-1}.

$$N(\Delta_x, \Delta_y) = N_0 \epsilon(\Delta_x, \Delta_y),$$

where

$$N_0 = \frac{P_\ell N_e \lambda f(\omega) \sigma_T}{hc^2}, \quad (18)$$

P_ℓ is the instantaneous laser power at the laser-electron IP, and N_e is the number of electrons in the bunch. If η_{det} is the detector efficiency then, using realistic numerical values, the number of detected photons is $N_{\mathrm{det}} \epsilon(\Delta_x, \Delta_y)$, where

$$N_{\mathrm{det}} = 1212 \times \xi \quad (19)$$

and

$$\xi = \frac{\eta_{\mathrm{det}}}{0.05} \frac{P_\ell}{10 \text{ MW}} \frac{N_e}{2 \times 10^{10}} \frac{\lambda}{532 \text{ nm}} \frac{f(\omega)}{0.2} \ \mu\text{m}. \quad (20)$$

2. Conventions for laser optics

In the following, the conventions used define z along the electron beam direction, y along vertical, and x along the laser-beam direction. The light intensity of the laser has the form

$$I_\ell(x, y, z) = \frac{I_0}{2\pi\sigma_\ell^2} \frac{1}{f_R(x)} \exp\left[-\frac{y^2 + z^2}{2\sigma_\ell^2 f_R(x)}\right] \qquad (21)$$

$$f_R(x) = 1 + \left(\frac{x}{x_R}\right)^2 \qquad (22)$$

$$\sigma_\ell = M^2\sigma_0 \quad \text{where } \sigma_0 = \lambda f_\# \qquad (23)$$

$$x_R = M^2\frac{4\pi\sigma_0^2}{\lambda}, \qquad (24)$$

where λ is the laser wavelength and M^2 is a quality factor for the laser, which effectively increases the wavelength $\lambda \to M^2\lambda$ compared to the diffraction limited case; an

ideal single-mode laser would have $M^2 = 1$. x_R is the Rayleigh range of the setup and $f_\#$ is the f-number of the optics, $f_\# = D_\ell/F$, where D_ℓ is the diameter of the lens and F is its focal length.

As in Ref. [29], 99% of energy in the Gaussian beam profile is required to be contained within the lens aperture. For the TM$_{00}$ mode this requirement means

$$0.99 = \int_0^{D/2} \int_0^{2\pi} rdrd\phi \frac{1}{2\pi\sigma_\ell^2} \exp\left[-\frac{r^2}{2\sigma_\ell^2}\right]$$

so $D \simeq 2 \times \pi\sigma_\ell$ and hence

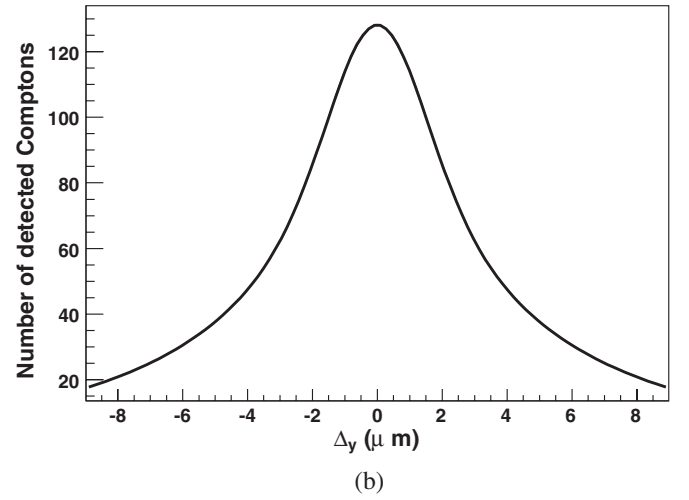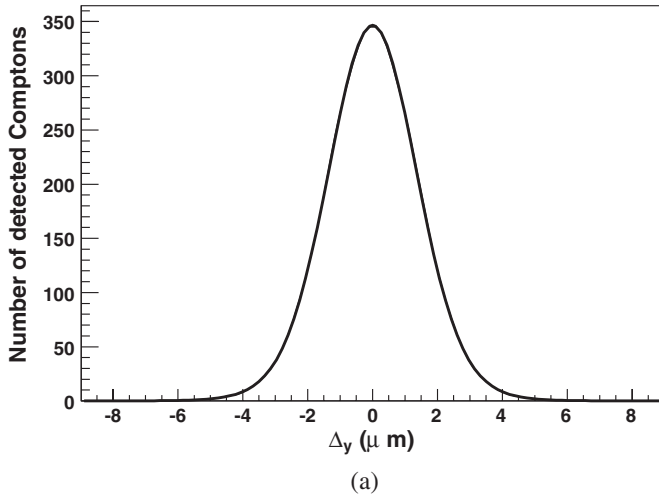$$\sigma_0|_{\text{TM}_{00}} = \lambda f_\#. \qquad (25)$$

(a)

(b)

FIG. 12. Scan profile at the laser-wire IP for a laser with $M^2 = 1.3$ and wavelength 532 nm operating in the TM$_{00}$ mode and focused using f_1 optics. The electron bunch is assumed to have a Gaussian transverse profile. (a) $\sigma_{ey} = 1~\mu$m, $\sigma_{ex} = 10~\mu$m. (b) $\sigma_{ey} = 1~\mu$m, $\sigma_{ex} = 100~\mu$m.
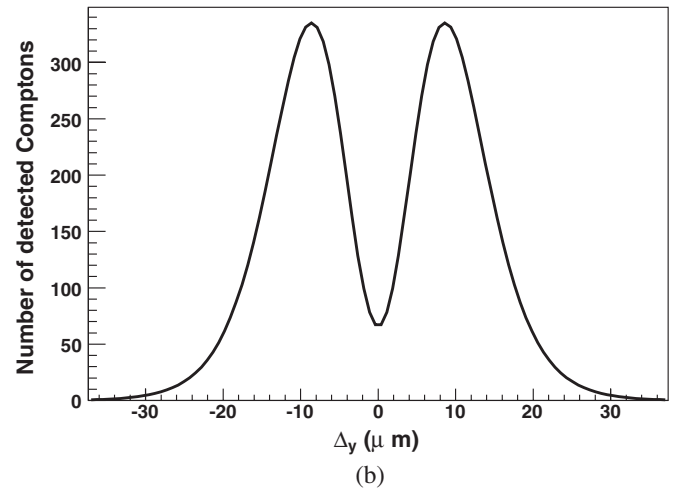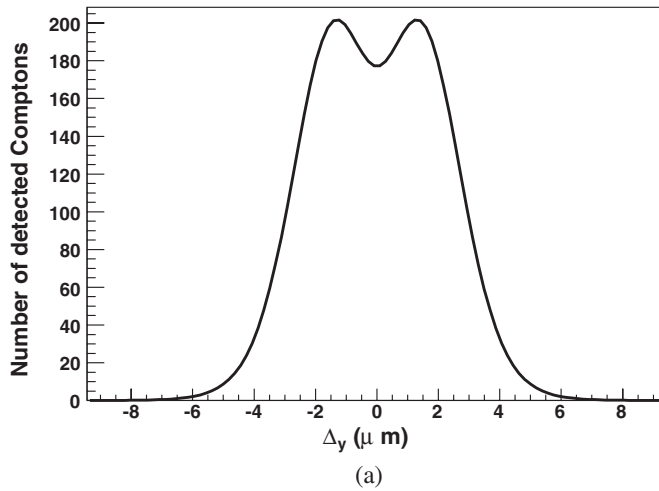

(a)

(b)

FIG. 13. Scan profile at the laser-wire IP for a laser with $M^2 = 1.3$ and wavelength 532 nm operating in the TM$_{01}$ mode and focused using f_1 optics. The electron bunch is assumed to have a Gaussian profile. (a) $\sigma_{ey} = 1~\mu$m, $\sigma_{ex} = 10~\mu$m. (b) $\sigma_{ey} = 5~\mu$m, $\sigma_{ex} = 50~\mu$m.

TABLE IV. Optimal f-numbers (for E_{stat}) and corresponding statistical precision for electron bunches with aspect ratio $\sigma_{ex}/\sigma_{ey} = 10$, $\lambda = 532$ nm. The laser $M^2 = 1.3$ for both TM_{00} and TM_{01} modes. The minimum practical f-number is taken as 1.0, even where a better statistical precision could in principle be obtained by smaller f-numbers. The factor of 1.15 of Eq. (A11) is included in the TM_{01} calculations. Also shown is the error E_{M^2} if there is a 5% error in the value of the laser M^2.

		TM_{00}			TM_{01}	
σ_{ey} (μm)	$f_\#$	$E_{\text{stat}}\%$	$E_{M^2}\%$	$f_\#$	$E_{\text{stat}}\%$	$E_{M^2}\%$
1	1	4.28	2.48	1	3.40	4.54
2	1.46	4.27	1.31	1.61	2.18	2.74
3	2.01	4.53	1.11	2.35	1.73	2.45
4	2.30	4.72	0.81	3.13	1.48	2.32
5	2.45	4.96	0.59	3.91	1.32	2.23
6	2.68	5.38	0.49	4.69	1.21	2.18
7	2.94	5.64	0.43	5.48	1.11	2.14
8	3.14	5.89	0.38	6.30	1.04	2.14
9	3.29	6.13	0.33	7.11	0.98	2.13
10	3.41	6.37	0.29	7.91	0.93	2.12

In this case, the opening angle $\theta = 1/f_\#$ between the center of the diverging Gaussian beam and its e^{-2} intensity cone is given by

$$\theta = \frac{\lambda}{\pi\sigma} = \frac{1}{f_\#}$$

and so, for TM_{00} with f_1 optics, $\sigma_0 = \lambda/\pi$ and $\theta = 1$ rad, or 57°.

3. Numerical results

Results for the case of laser-$M^2 = 1.3$ and f_1 final-focus optics are shown in Fig. 12 for an electron-bunch trans-verse Gaussian profiles with (a) $\sigma_{ey} = 1$ μm, $\sigma_{ex} = 10$ μm and (b) $\sigma_{ey} = 1$ μm, $\sigma_{ex} = 100$ μm; the effect of the Rayleigh range is very apparent for the larger aspect ratio.

Results for the case of operating the laser in TM_{01} mode with laser-$M^2 = 1.3$ and f_1 final-focus optics are shown in Fig. 13 for electron-bunch transverse Gaussian profiles with (a) $\sigma_{ey} = 1$ μm, $\sigma_{ex} = 10$ μm and (b) $\sigma_{ey} = 5$ μm, $\sigma_{ex} = 50$ μm; the potential benefit of the TM_{01} mode is apparent for the larger vertical spot size. The relative benefits of the TM_{00} and TM_{01} modes are pre-sented in Table IV, where it can be seen that for $\sigma_{ey} > 1$–2 μm there is a significant advantage for the statistical power by using the TM_{01} mode; this advantage has been demonstrated at the ATF [30]. However, the sensitivity to the laser properties (as parametrized by a simple M^2 in these calculations) is greater for the TM_{01} mode and, for spot sizes of order 1 μm, the relative statistical power of the TM_{01} to that of the TM_{00} mode decreases rapidly, as illustrated in Fig. 14. In this study, the laser-spot sizes of order 1 μm are of particular importance for the BDS LW system, so in the following the TM_{00} mode is used, while acknowledging that higher-order laser modes may be ad-vantageous in other locations.

4. Error contribution from the laser-wire scan

In this section the various contributions to the relative error E_{scan} in Eq. (8) are outlined. If σ_{scan} is the electron beam size after subtracting the laser effects discussed below, then

$$E_{\text{scan}} = \left(\frac{\sigma_{\text{scan}}}{\sigma_e}\right)^2 \frac{\delta\sigma_{\text{scan}}}{\sigma_{\text{scan}}}. \tag{26}$$
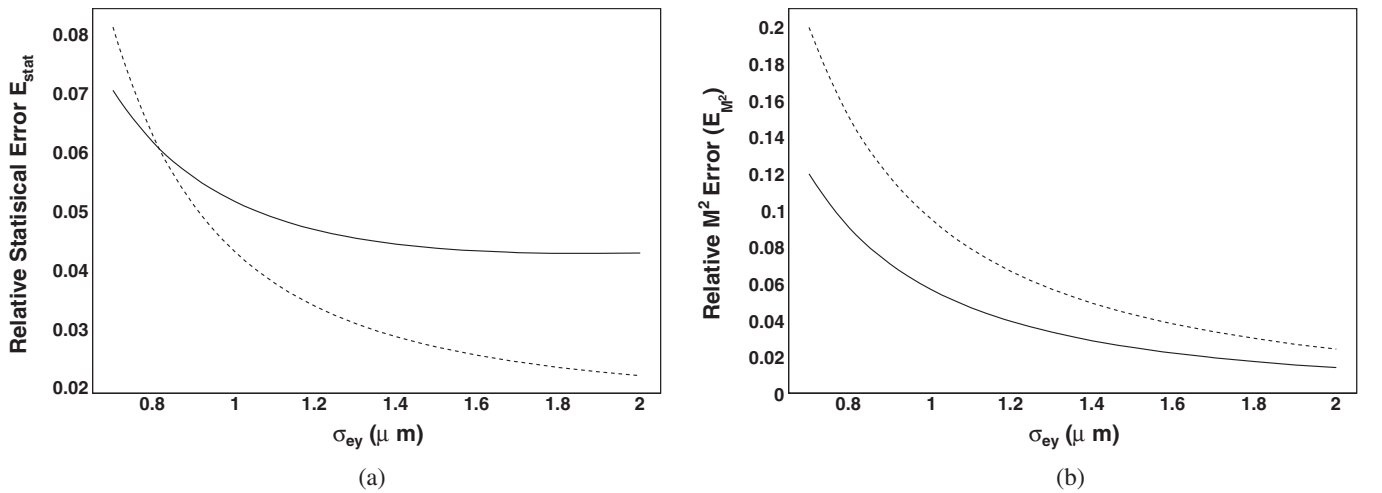
FIG. 14. Relative errors as a function of electron vertical Gaussian spot size, σ_{ey}, for scans using a laser with nominal $M^2 = 1.3$, wavelength 532 nm, operating in the TM_{00} mode (full lines) and TM_{01} mode (dashed lines). At each point, the value of final focusing $f_\#$ has been chosen to optimize the statistical error. (a) statistical error E_{stat}. (b) relative change, E_{M^2}, in the extracted value of σ_{ey} arising from a 5% error in the value of the laser M^2.

σ_{scan} itself is obtained from subtracting the effects of the laser pointing instability,

$$\sigma_{\text{scan}} = [\sigma_{\text{fit}}^2 - \sigma_{\text{point}}^2]^{1/2}, \qquad (27)$$

where σ_{fit} is the raw result of a fit to the laser-wire scan profile, for which the errors are discussed in detail in Sec. III B. σ_{point} is the contribution to the scan profile from the rms laser pointing angular fluctuations ψ_ℓ; $\sigma_{\text{point}} = F\psi_\ell$, where F is the focal length of the lens. As discussed in Sec. III C 1 $F \geq 15$ mm.

After subtracting σ_{point} as in Eq. (27), the error contribution can thus be written as

$$\frac{\delta\sigma_{\text{scan}}^2}{\sigma_{\text{scan}}^2} = E_{\text{fit}}^2 + E_{\text{point}}^2, \qquad (28)$$

where

$$E_{\text{fit}} = \left(\frac{\sigma_{\text{fit}}}{\sigma_{\text{scan}}}\right)^2 \frac{\delta\sigma_{\text{fit}}}{\sigma_{\text{fit}}} \qquad (29)$$

and

$$E_{\text{point}} = \left(\frac{F\psi}{\sigma_{\text{scan}}}\right)^2 \frac{\langle\delta\psi\rangle}{\psi}, \qquad (30)$$

where $\langle\delta\psi\rangle$ is the resolution of the measurement of the rms pointing stability. Inserting the nominal practical values $F = 15$ mm, $\psi = 10$ μrad, $\mu = 1$ μm, and $\langle\delta\psi\rangle/\psi = 0.1$ gives $E_{\text{point}} \simeq 2.24 \times 10^{-3}$.

B. Laser-wire performance

In this section the performance of the ILC laser-wire systems will be examined in detail with a view to quantifying the errors that contribute to $\delta\sigma_{\text{fit}}$ of Eq. (29). The contributions to the raw laser-wire scan can be broken down as follows:

$$\left(\frac{\delta\sigma_{\text{fit}}}{\sigma_{\text{fit}}}\right)^2 = \frac{19}{N_{\text{scan}}}\left(\frac{E_{\text{stat}}}{\sqrt{\xi}} + E_\xi\right)^2 + E_{M^2}^2, \qquad (31)$$

where E_{stat} is the statistical error of a 19-point fit to the raw scan curve (Sec. III C 1). In general, N_{scan} laser shots could be used in a variety of scanning modes. However, as set examples in this paper, all the scans consist of $N_{\text{scan}} = 19$ equally spaced values of Δ_y over a range $\pm 7\sigma_m$ [as defined in Eq. (A4)], with $\Delta_x = 0$ and $\xi = 1.0$, where ξ is as defined in Eq. (20). E_ξ is the error arising from the shot-by-shot normalization fluctuations as introduced in Eq. (37).

E_{M^2} is the error on the extraction of σ_e introduced by the error on the laser light distribution at the IP; this is characterized here by an error in the M^2 value of the laser and, for a real system, will need to be calculated including the effects of alignment errors, etc. in the final-focus optics. As illustrated in Sec. III C 1 E_{M^2} can be estimated by fitting the measured profile to σ_{ey} assuming a value of M^2 that is wrong by a factor $(1 + \delta_{M^2})$. In the following, the laser M^2

is thus assumed to be determined shot by shot to an accuracy of δ_{M^2}. Naively, without allowing for Rayleigh-range effects, the error on the extracted value of σ_e from subtraction of the laser spot size is

$$\frac{\delta\sigma_e}{\sigma_e} = \frac{\sigma_\ell}{\sigma_e^2}\delta\sigma_e \simeq \left(\frac{\lambda f_\#}{\sigma_e}\right)^2 M^2 \delta_{M^2}. \qquad (32)$$

Inserting the representative values of $M^2 = 1.3$ and $\sigma_e = 1$ μm gives

TABLE V.   Optimal f-numbers (for E_{stat}) for the measurement of σ_{ey} and the corresponding statistical precision for $\sigma_{ey} = 1$ μm, $\lambda = 532$ nm, and $M^2 = 1.3$. The minimum practical f-number is taken as 1.0, even where a better statistical precision could in principle be obtained by smaller f-numbers. The numbers in brackets are the corresponding statistical errors using $f_{1.5}$ optics; the systematic errors due to $\delta_{M^2} = 0.01, 0.05, 0.10$ are then 1.09%, 5.68%, and 12%, respectively, and do not depend significantly on the electron-bunch aspect ratio.

σ_{ex}/σ_{ey}	Optimal $f_\#$	E_{stat} (%)	E_{M^2} (%) for $\delta_{M^2} =$
			0.01	0.05	0.10
1	1	2.93 (4.47)	0.48	2.48	5.16
2	1	2.97 (4.49)	0.48	2.48	5.16
5	1	2.48 (4.62)	0.48	2.48	5.16
10	1	4.28 (5.15)	0.48	2.48	5.16
15	1.10	5.49 (6.00)	0.58	3.01	6.27
20	1.19	6.72 (7.01)	0.68	3.54	7.40
25	1.26	7.91 (8.10)	0.76	3.96	8.30
50	1.35	13.6 (13.7)	0.89	4.60	9.68
100	1.25	23.5 (23.9)	0.76	3.93	8.24

TABLE VI.   Optimal f-numbers (for E_{stat}) for the measurement of σ_{ey} and the corresponding statistical precision for $\sigma_{ey} = 1$ μm, $\lambda = 355$ nm, and $M^2 = 1.3$. The minimum practical f-number is taken as 1.0, even where a better statistical precision could in principle be obtained by smaller f-numbers. The numbers in brackets are the corresponding statistical errors using $f_{1.5}$ optics; the systematic errors due to $\delta_{M^2} = 0.01, 0.05, 0.10$ are then 0.48%, 2.48%, and 5.16%, respectively, and do not depend significantly on the electron-bunch aspect ratio.

σ_{ex}/σ_{ey}	Optimal $f_\#$	E_{stat} (%)	E_{M^2} (%) for $\delta_{M^2} =$
			0.01	0.05	0.10
1	1	3.17 (4.05)	0.21	1.10	2.26
2	1	3.23 (4.08)	0.21	1.10	2.26
5	1	3.62 (4.25)	0.21	1.10	2.26
10	1.23	4.76 (4.92)	0.33	1.69	3.48
15	1.44	5.92 (5.93)	0.44	2.28	4.72
20	1.58	7.06 (7.07)	0.54	2.77	5.76
25	1.69	8.19 (8.27)	0.61	3.17	6.62
50	1.97	13.7 (14.2)	0.83	4.31	9.05
100	1.97	23.9 (24.5)	0.83	4.31	9.05

I. AGAPOV, G. A. BLAIR, AND M. WOODLEY

Phys. Rev. ST Accel. Beams **10,** 112801 (2007)

TABLE VII. Optimal f-numbers (for E_{stat}) for the measurement of σ_{ey} and the corresponding statistical precision for $\sigma_{ey} = 1~\mu m$, $\lambda = 266$ nm, and $M^2 = 1.3$. The minimum practical f-number is taken as 1.0, even where a better statistical precision could in principle be obtained by smaller f-numbers. The numbers in brackets are the corresponding statistical errors using $f_{1.5}$ optics; the systematic errors due to $\delta_{M^2} = 0.01, 0.05, 0.10$ are then 0.27%, 1.39%, and 2.87%, respectively, and do not depend significantly on the electron-bunch aspect ratio.

	Optimal		E_{M^2} (%) for $\delta_{M^2} =$		
σ_{ex}/σ_{ey}	$f_\#$	E_{stat} (%)	0.01	0.05	0.10
1	1	3.64 (4.25)	0.12	0.61	1.26
2	1	3.71 (4.27)	0.12	0.61	1.26
5	1.07	4.19 (4.49)	0.14	0.71	1.45
10	1.46	5.30 (5.31)	0.26	1.31	2.71
15	1.72	6.41 (6.49)	0.36	1.83	3.78
20	1.91	7.51 (7.80)	0.44	2.26	4.69
25	2.06	8.59 (9.16)	0.51	2.65	5.50
50	2.31	14.0 (15.8)	0.64	3.33	6.95
100	2.27	24.4 (27.2)	0.62	3.22	6.68

$$\frac{\delta\sigma_e}{\sigma_e} = 1.08\left[\left(\frac{M^2}{1.3}\right)\left(\frac{1~\mu m}{\sigma}\right)\left(\frac{\lambda}{532~\text{nm}}\right)\left(\frac{f_\#}{1.5}\right)\right]^2\delta_{M^2}. \quad (33)$$

A full numerical treatment, using the relations given in Appendix A, is presented in Tables V, VI, and VII and shows that this is a good approximation for small $\delta_{M^2} \simeq 1\%$ but is a slight underestimate for larger values.

C. Statistical errors from the laser-wire fits

1. Fits to TM_{00} distributions

The overlap integrals necessary to calculate the number of LW Compton photons are presented in Appendix A. A numerical evaluation of Eq. (A2) is now used to simulate

laser-wire scans for a variety of situations of interest to the ILC.

Both E_{stat} and E_{M^2} will depend on the f-number of the laser optics employed. This dependence is illustrated in Fig. 15 for the case of $\sigma_{ey} = 1~\mu m$ and $\sigma_{ex} = 25~\mu m$. For each set of σ_{ex}, σ_{ey}, there is an optimal f-number that gives the lowest statistical error for given values of ξ and N_{scan}. However, as can be seen in Fig. 15, the minima are often fairly shallow, which must be contrasted with the difficulty of building low f-number optics. The difficulty is not just in building low f-number alone, but in producing a system that can maintain a small laser spot size approximately $\pm 10\sigma_\ell$ off axis, as needed during a scan. For this reason, f-numbers less than 1 are not considered here. In addition to determining the optimal f-number for various electron transverse dimensions, the nominal errors E_{stat} and E_{M^2} are also determined here for $f_{1.5}$ optics, because this is a likely technological goal for a system that will produce a small spot size both on the optical axis and over an acceptable scan range of order 1 mrad.

The beam pipe in the ILC BDS has inner radius of 12 mm and outer radius of approximately 14 mm. In order to ensure sufficient clearance from the beam halo, the minimum focal length is taken here to be $F_{min} = 15$ mm. Imposing the requirement of being able to scan $\pm 7\sigma_m$, then the scanning system must be able to scan a range

$$\theta_{scan} \geq \frac{7\sigma_m}{F_{min}}. \quad (34)$$

Imposing this condition on the most challenging small spot size of $\sigma_{ey} = 1~\mu m$, $\sigma_\ell = 1~\mu m$ (assuming $M^2 = 1.3$ and so $\sigma_m \simeq 1.4~\mu m$ gives $\theta_{scan} \gtrsim 0.7$ mrad. The maximum scanning rate will depend on the scan range required so, with this in mind, the scan range should be kept as small as practical. In the following the condition
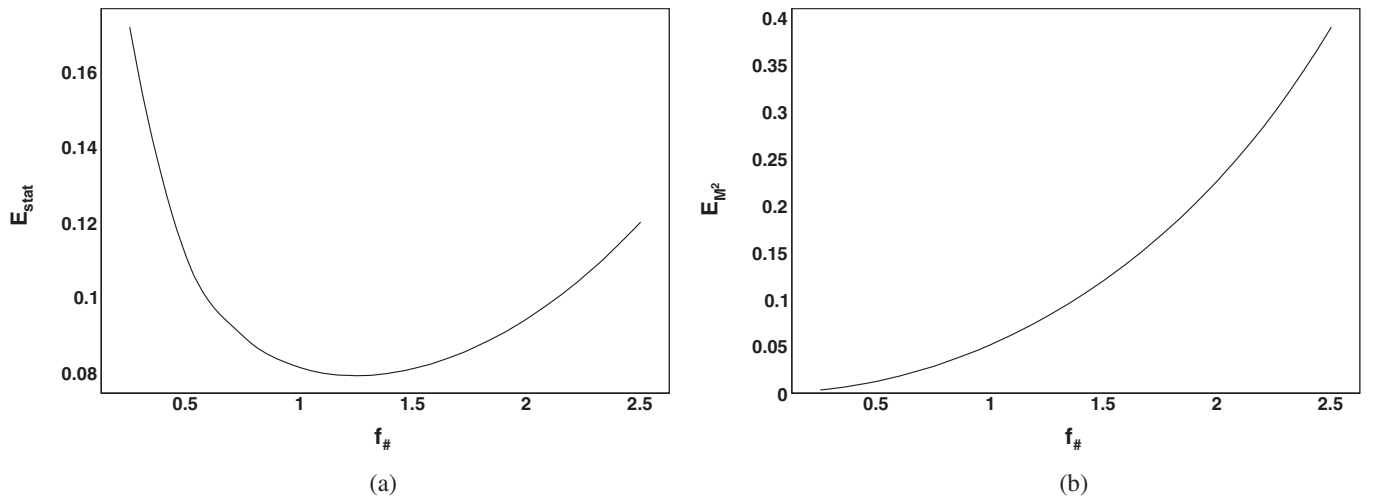

(a)

(b)

FIG. 15. (a) Statistical error E_{stat}, (b) laser error E_{M^2} for $\xi = 1$ [Eq. (20)] using $N_{scan} = 19$ scan points versus the f-number of the final-focus lens, using a laser with $M^2 = 1.3$ and operating in the TM_{00} mode with $\lambda = 532$ nm. The electron bunch is assumed to have a Gaussian transverse profile with $\sigma_{ey} = 1~\mu m$ and $\sigma_{ex} = 25~\mu m$.

$$\theta_{\text{scan}}^{\max} \simeq 1 \text{ mrad} \qquad (35)$$

is therefore adopted. For larger spot sizes and for the horizontal (or skew angle) scans of the electron bunch, the suitable f-number is determined primarily by the angular scan range of the final-focus lens plus scanning system. The laser optics for these dimensions will probably use diameter $D = 5$ cm optics (or similar). In this case, assuming again a scan range of $7\sigma_m$ the practical $f_\#$ is given by

$$f_\# = 1.4\left(\frac{\sigma_m}{10 \ \mu\text{m}}\right)\left(\frac{5 \text{ cm}}{D}\right)\left(\frac{1 \text{ mrad}}{\theta_{\text{scan}}^{\max}}\right). \qquad (36)$$

The errors obtained from a laser-wire scan using an $f_\#$ given by Eq. (36) for the horizontal dimension σ_{ex} are given in Table VIII. In practice, for very large scan ranges, it may be preferable to use a stepping-motor system to move the final-focus lens as opposed to scanning using optical ray deflection, which would enable smaller $f_\#$s to be employed. In that case, the scan would have to be very slow compared to the machine repetition rate.

2. Normalization fluctuations

The error on the normalization factor ξ is given by

$$\frac{\delta\xi}{\xi} = \left[\left(\frac{\delta P_\ell}{P_\ell}\right)^2 + \left(\frac{\delta N_e}{N_e}\right)^2 + \left[\frac{\delta\xi}{\xi}\right]_T^2\right]^{1/2}, \qquad (37)$$

where δP_ℓ is the resolution of the measured laser power, δN_e is the bunch charge measurement resolution, and the final term is the contribution from time jitter (or phase error) between the laser and electron beams.

The laser power can be measured bunch-by-bunch by a fast photodiode presumably to a level of order 10^{-2} and the bunch charge to a similar level by using dedicated current monitors or by combining measurements from a set of BPMs.

TABLE VIII. Errors for the scan of the horizontal dimension σ_{ex} for various aspect ratios σ_{ex}/σ_{ey} when $\sigma_{ey} = 1 \ \mu\text{m}$. The f-numbers are chosen so that the angular scanning range can be limited to 1 mrad; the f-number used is given by whichever is the greater of 1.5 and the value given by Eq. (36). The laser properties assumed are $\lambda = 532$ nm and $M^2 = 1.3$.

| | Practical | | E_{M^2} (%) for $\delta_{M^2} =$ | | |
σ_{ex}/σ_{ey}	$f_\#$	E_{stat} (%)	0.01	0.05	0.10
1	1.5	4.47	1.09	5.68	12.0
2	1.5	3.41	0.27	1.39	2.86
5	1.5	4.22	0.04	0.22	0.45
10	1.5	5.74	0.01	0.06	0.11
15	2.1	7.02	0.01	0.05	0.10
20	2.8	8.10	0.01	0.05	0.10
25	3.5	9.06	0.01	0.05	0.10
50	7.0	12.8	0.01	0.05	0.10
100	14	18.1	0.01	0.05	0.10

The contribution from time jitter is now addressed. As indicated in Table I, the ILC bunch train consists of $N_{\text{train}} = 2625$ bunches with repetition frequency $f_{\text{rep}} = 5$ Hz. Each bunch has length $L_b = 300 \ \mu\text{m}$ with corresponding bunch Gaussian time width of $T_b = L_b/c = 1$ ps.

If T_ℓ is the laser pulse length and τ_ℓ is the rms time jitter between the laser and electron pulses, then the rms contribution of this temporal fluctuation to the relative value of the overlap integral of Gaussian laser and electron profiles is given by

$$\left[\frac{\delta\xi}{\xi}\right]_T = \frac{1}{\sqrt{2}}\frac{\tau_\ell^2}{T_\ell^2 + T_b^2} \qquad (38)$$

or after including typical ILC values

$$\left[\frac{\delta\xi}{\xi}\right]_T = 1.80 \times 10^{-2}\left(\frac{\tau_\ell}{0.3 \text{ ps}}\right)^2\left[\left(\frac{T_\ell}{2 \text{ ps}}\right)^2 + \left(\frac{T_b}{1 \text{ ps}}\right)^2\right]^{-1}. \qquad (39)$$

The number of Compton photons [Eq. (18)] produced by each laser shot is proportional to the instantaneous value of ξ and so any shot-by-shot ξ-fluctuations will contribute to the error on the fit to the raw LW scan, as given by

$$\Delta N = \left[N\left(1 + \frac{\langle\delta\xi\rangle}{\xi}N\right)\right]^{1/2}. \qquad (40)$$

Performing the fit with this additional error factor enables its contribution to the total error [Eq. (31)] to be determined according to

$$E_\xi = a_\xi\frac{\langle\delta\xi\rangle}{\xi}, \qquad (41)$$

where values of the coefficient a_ξ are given in Table IX for a range of electron-bunch vertical spot sizes and aspect ratios σ_{ex}/σ_{ey}. Combining all the terms, the normalization error as given by Eqs. (37) and (41) becomes

$$E_\xi \simeq 2.3 \times 10^{-2}a_\xi. \qquad (42)$$

TABLE IX. The factor a_ξ defined in Eq. (41) for a set of electron beam sizes of interest at the ILC. Laser wavelength = 532 nm, $M^2 = 1.3$, f-num = 1.5.

| σ_{ey} | | | σ_{ex}/σ_{ey} | | | | |
(μm)	1	2	5	10	15	20	25
1	0.05	0.05	0.06	0.13	0.27	0.43	0.60
2	0.03	0.03	0.04	0.12	0.25	0.38	0.50
3	0.03	0.03	0.04	0.12	0.24	0.36	0.48
4	0.03	0.03	0.04	0.12	0.24	0.36	0.47
5	0.03	0.03	0.04	0.12	0.24	0.35	0.47

3. Alternative scanning mode

An alternative laser-wire scanning mode can be considered where the laser is kept fixed in space relative to the center of an accurate BPM. The relative offset Δ_y between the laser and the electron bunch can then be measured by the BPM on a bunch-by-bunch basis to an accuracy given by the BPM resolution σ_{BPM}.

If the bunch charge N_e and laser power P_ℓ are also measured on a bunch-by-bunch basis, then the factor ξ defined in Eq. (20) is known to an accuracy given by Eq. (37). If it is assumed that the electron transverse charge distribution is a pure Gaussian, then Eq. (A2) can be inverted bunch by bunch.

Given that Δ_y is generated by the bunch jitter with rms value $\alpha_J \sigma_{ey}$ and assuming $\sigma_{ey} \simeq \sigma_\ell \simeq \sigma_m/\sqrt{2} \simeq 1~\mu\mathrm{m}$ and $\alpha_J \simeq 0.25$, then typical values of N_{det} [Eq. (19)] are of order

$$N_{\mathrm{det}} = \xi \frac{1212}{2\sqrt{\pi}\sigma_{ey}} \left\langle \exp - \frac{\Delta_y^2}{4\sigma_{ey}^2} \right\rangle \simeq \frac{342}{\sqrt{1 + 0.5\alpha_J^2}} \simeq 332, \tag{43}$$

giving a statistical error on each measured value of N of order 5%. In addition there will be a contribution to the error from ξ due to the measurements of bunch charge and laser power and from the laser trigger (phase) jitter. In the following, the total error on ξ is taken to be 2%. The expected measurement error on the transverse size σ_{ey} of the electron bunch was then evaluated for a nominal electron spot size of $\sigma_{ey} = 1~\mu\mathrm{m}$ by $\sigma_{ex} = 10~\mu\mathrm{m}$ by inverting the full overlap integral of Eq. (A2).

The resulting percentage error on a single-shot measurement of σ_{ey} is presented in Fig. 16 as a function of (a) BPM resolution and (b) rms beam jitter α_J. From these plots it can be deduced that the bunch-by-bunch error on σ_{ey} is of order 15% for the chosen realistic parameters. Making such measurements over a whole train would then yield an error on the average spots size of the train of $0.15/\sqrt{2625} \simeq 2.9 \times 10^{-3}$.

D. Summary of laser-wire requirements

A LW system for the ILC BDS will involve many sophisticated elements including high-power mode-locked lasers, high quality laser final-focus optics, and integrated BPM systems. In this section, the desired performance specifications of the key subsystems are discussed and the resulting errors on the measured electron transverse spot-size are estimated.

1. Laser requirements

The above analysis has discussed various laser requirements that must be met if fast intratrain emittance measurements are to be performed at the ILC. These requirements are gathered here to provide a benchmark for R&D requirements [31] and to act as a baseline for subsequent discussion of the other laser-wire component specifications.

The laser supplying the light to the laser-wire IP will need to match the ILC bunch structure, providing laser pulses each of instantaneous power $P_\ell \simeq 10~\mathrm{MW}$ with sufficient pulse length to overlap fully with the electron bunch so as to minimize any synchronization issues.

The pulse pattern and synchronization can be obtained by mode locking a master laser oscillator to a subharmonic of the machine radio frequency and then by pulse picking for high-power amplification. Assuming that only the re-
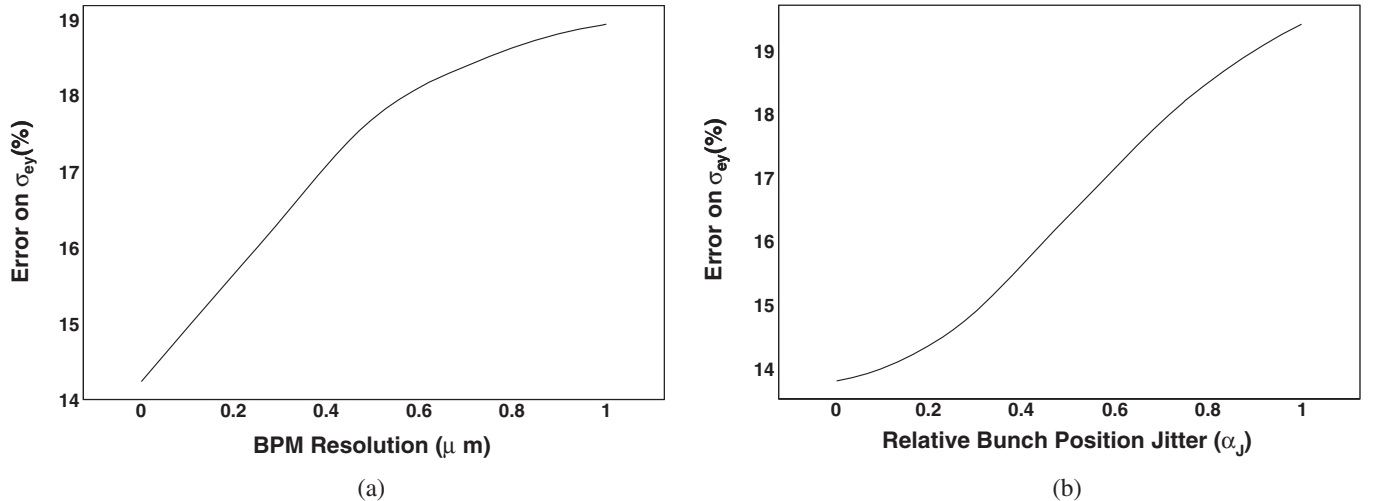

FIG. 16.   Percentage errors obtained by inverting Eq. (A2) on a bunch-by-bunch basis for electron-bunch transverse dimensions $\sigma_{ey} = 1~\mu\mathrm{m}$, $\sigma_{ex} = 10~\mu\mathrm{m}$, laser wavelength $= 532$ nm, $M^2 = 1.3$, f-num $= 1.5$, $P_\ell = 10~\mathrm{MW}$. (a) As a function of BPM resolution (in $\mu\mathrm{m}$) with the relative beam jitter fixed at $\alpha_J = 0.25$. (b) As a function of beam jitter (α_J) with the BPM resolution fixed at 0.1 $\mu\mathrm{m}$.

quired pulses are amplified, the average power of the laser will be dominated by only those amplified pulses and so can be estimated as

$$P_\ell^{av} = 0.5 \text{ W} \times \left(\frac{N_{train}}{2625}\right)\left(\frac{f_{rep}}{5 \text{ Hz}}\right)\left(\frac{P_\ell}{20 \text{ MW}}\right)\left(\frac{T_\ell}{2 \text{ ps}}\right), \quad (44)$$

where f_{rep} is the repetition rate of the machine (Table I). If no pulse picking for the high-power pulses were applied, then P_ℓ^{av} would be 108 W, assuming the ILC nominal bunch spacing of 369 ns (Table I), which would make the laser very much more challenging. An extra factor of 2 has been included in the laser power requirements for P_ℓ, because at the ILC the light transport between laser and IP may be as long as several hundred meters and so will involve substantial power losses en route.

2. Error summary

The most challenging laser-wire measurements at the ILC occur in the BDS and some representative values of the bunch dimensions of interest are given in Table II. For illustration in this table, the precisions obtainable on the matrix element $\langle xy \rangle$ are listed, assuming that each dimension σ_x, σ_y, and σ_u can be measured to a nominal 1% (which means σ_x^2 and σ_y^2 are measured to 2%). Some examples of vertical emittance reconstructions for 4D optics using these assumptions are presented in Figs. 17 and 18.

In order to summarize the ILC laser-wire requirements and to describe the various contribution to the measurement errors, a beam with representative transverse dimensions $\sigma_{ex} = 10 \ \mu\text{m} \times \sigma_{ey} = 1 \ \mu\text{m}$ is now used as a specific example to illustrate the key points. This beam is somewhat more challenging than that expected at the nominal ILC, but points to where additional R&D may
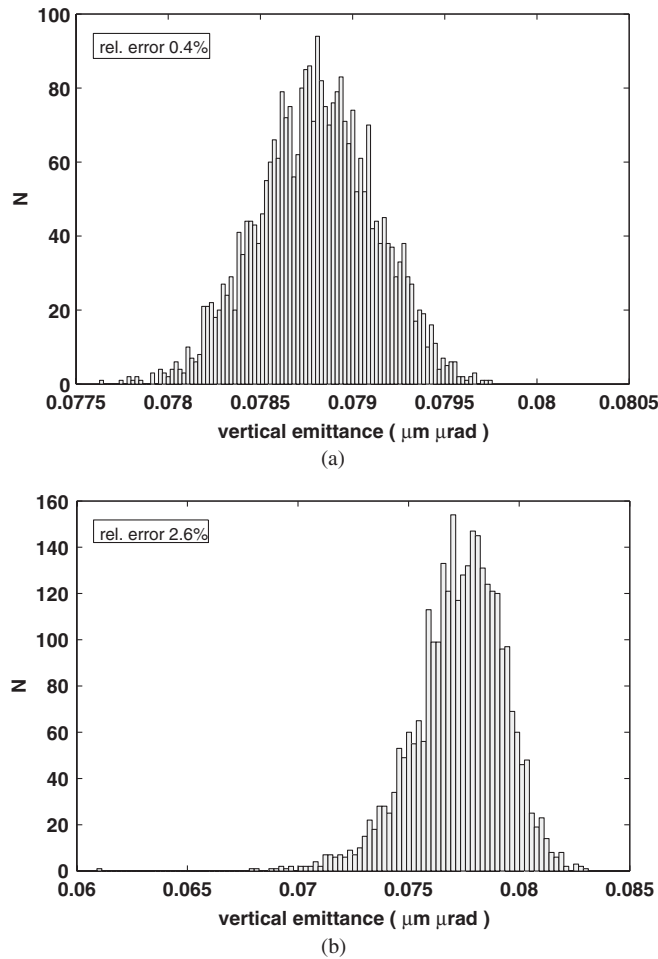

FIG. 17.   Distribution of reconstructed vertical emittance with 1% (a) and 5% (b) random errors on the beam size measurement for a 4D diagnostics section (statistics corresponding to train length). Initial optical functions are perfectly matched. The true emittance is 0.079 μm · μrad.
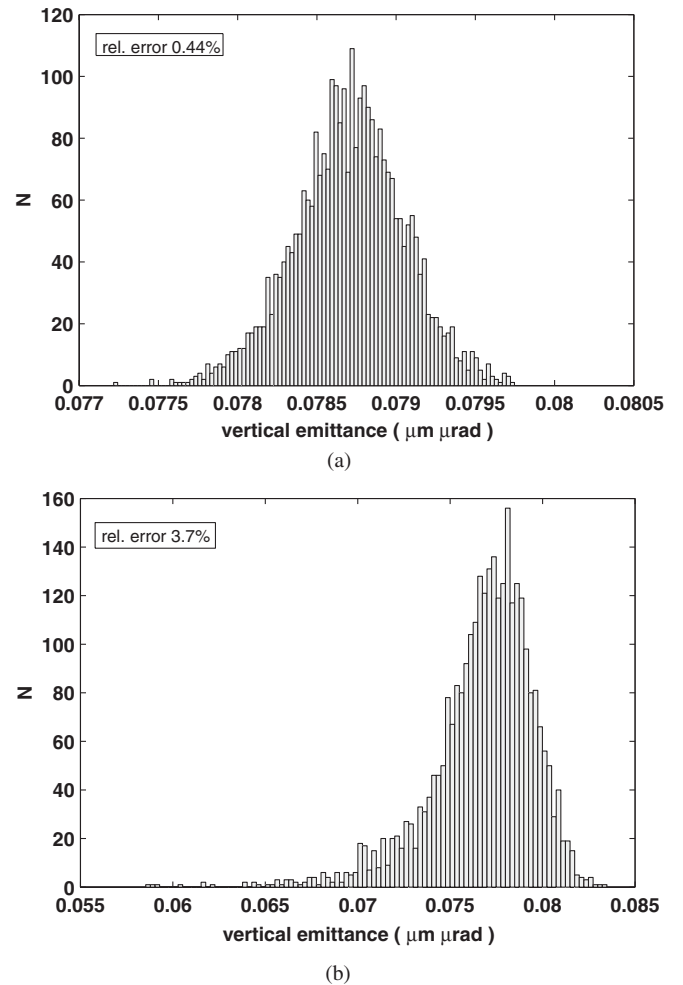
FIG. 18.   Distribution of reconstructed vertical emittance with 1% (a) and 5% (b) random errors on the beam size measurement for a 4D diagnostics section assuming 50% random mismatch of initial optical functions (statistics corresponding to train length). The true emittance is 0.079 μm · μrad.

I. AGAPOV, G. A. BLAIR, AND M. WOODLEY

Phys. Rev. ST Accel. Beams **10,** 112801 (2007)

TABLE X. Requirements on laser system for intratrain laser-wire scans at the ILC, with reference to the equation that sets the goal value. Note, an extra factor of 2 has been applied to allow a 50% loss of power due to light transport between the laser and the laser-wire IP, which may involve distances of several hundred meters in the ILC.

Parameter	Symbol	Goal value	Equation
Wavelength	λ	≤ 532 nm	(23)
Mode quality	M^2	≤ 1.3	(23)
Peak power	P_ℓ	≥ 20 MW	(18)
Average power	P_ℓ^{av}	≥ 0.5 W	(44)
Pulse length	T_ℓ	≥ 2 ps	(39)
Trigger stability	τ_ℓ	≤ 0.3 ps	(39)
Pointing stability	ψ_ℓ	≤ 10 μrad	(30)

be required if specific operating conditions give rise to smaller spot sizes.

The following laser, optical, and BPM specifications are nontrivial and are themselves subjects of R&D, however it is probable that suitable solutions to them will be found. The assumptions are:

(i) the laser requirements of Table X can be met,
(ii) the bunch-by-bunch charge and the laser instantaneous power can both be measured to 10^{-2},
(iii) the laser profile at the IP (characterized in this paper by a simple M^2 value) is known to the equivalent of $\delta_{M^2} = 0.01$,
(iv) BPM resolution $\sigma_{BPM} = 20$ nm.
(v) $f_{1.5}$ optics can be made to work, together with the scanning system.

All the errors discussed above are summarized in Table XI for the most challenging nominal transverse

TABLE XI. Error terms for σ_{ey} for an electron bunch whose transverse dimensions are $\sigma_{ey} = 1$ μm and $\sigma_{ex} = 10$ μm, giving $\sigma_u = 1.41$ μm and $\sigma_v = 9.95$ μm. The values were obtained assuming the performance goals of Table X, laser $\delta_{M^2} = 0.01$, $\sigma_{BPM} = 20$ nm, $\alpha_J = 0.25$, The electron-bunch charge and laser power are assumed each to be known to 1% and the pointing jitter to 10%. The measurement statistical errors are for a full train (i.e. $N_{scan} \simeq 140$). No subtraction of residual dispersion has been made for these measurements; instead they are input into the global fit to extract the emittance and dispersion terms together.

	Symbol	σ_y	σ_u	σ_x
Value (μm)	σ_e	1	1.41	10
Laser wavelength (nm)	λ	532 (266)	532 (266)	532
Optics f-number	$f_\#$	1.5	1.5	1.5
Optics focal length (mm)	F	15	15	70
Pointing stability ($\times 10^{-3}$)	E_{point}	2.2	1.1	0.5
Beam jitter ($\times 10^{-3}$)	E_{jitter}	5.0	3.5	0.5
Fit statistics ($\times 10^{-3}$)	E_{stat}	4.3 (4.5)	3.4 (4.2)	4.8
Laser spot size ($\times 10^{-3}$)	E_{M^2}	10.9 (2.7)	5.4 (1.4)	0.1
Normalization ($\times 10^{-3}$)	E_ξ	0.9 (0.6)	0.7 (0.5)	0.4
Total error ($\times 10^{-3}$)	$\delta\sigma/\sigma$	13.0 (7.6)	7.5 (5.8)	4.9

dimensions of interest to the ILC, namely: $\sigma_{ey} = 1$ μm, $\sigma_{ex} = 10$ μm, with corresponding skew scans with dimensions: $\sigma_u = 1.41$ μm and $\sigma_v = 9.95$ μm.

Note that in order to reduce the error from the laser-spot size uncertainty for the 1 μm vertical spot size, UV laser light ($\lambda = 266$ nm) has been used. In this case, additional laser power (perhaps by a factor of approximately 1.5–2) may be required to compensate for the inefficiency of the second laser frequency doubling. Most of this factor has already been included in the extra contingency factor of 2 discussed in Sec. III D 1.

IV. CONCLUSION

The measurement of emittance at the ILC will be essential to maintain the high luminosity performance of the machine. A fast noninvasive scheme to do this has been presented, which involves advanced laser-wire systems and dedicated machine optics. It was shown that the efficiency of emittance determination falls dramatically if the transverse electron-bunch measurements provide an accuracy worse than about 30%. The accuracy of the resulting emittance measurement is directly related to the transverse electron-bunch measurements; it is therefore preferable to achieve accurate profile measurements of order 1%–5%. A set of methods for emittance reconstruction was presented to improve the reconstruction efficiency in the event of degraded precision and a general scheme for the optics of the emittance measurement section was discussed.

The most challenging vertical spot sizes in the ILC BDS will eventually be of order 1 μm. The required LW performance was discussed in detail and a plausible route to obtaining a transverse spot-size measurement with a relative precision of order 1.3% using green laser light was presented, together with prospects of achieving modestly improved measurements using ultraviolet light. It can be concluded that, while percent-scale measurements on a train-by-train basis seem possible, many subsystems need significant improvements over the current state of the art; an ongoing program of R&D is currently addressing these challenges.

ACKNOWLEDGMENTS

APPENDIX A: LASER-WIRE OVERLAP INTEGRALS

In the following, the electron beam is assumed to have a simple Gaussian charge profile, with σ_{ex} and σ_{ey} being the

horizontal and vertical electron spot sizes, respectively. σ_z is assumed long compared to the laser spot size, so the overlap integral in z integrates out trivially.

1. Scans using the laser TM$_{00}$ mode

In this section, the full overlap integrals of TM$_{00}$ and TM$_{01}$ laser modes with a Gaussian electron bunch are presented, building on previous studies [32] by including full effects of Rayleigh range and detailed analysis of the laser final-focus optics. The results of the numerical integrals for a range of parameters of interest to ILC laser wires are presented in Tables V, VI, and VII.

For the laser TM$_{00}$ mode, after performing the z-integral, the remaining transverse overlap integral is

$$\epsilon(\Delta_x, \Delta_y) = \int \frac{dxdyI_\ell I_e}{(2\pi)^{3/2}\sigma_{ex}\sigma_{ey}\sigma_\ell\sqrt{f_R(x - \Delta_x)}}$$
$$\times \exp\left[-\frac{x^2}{2\sigma_{ex}^2} - \frac{y^2}{2\sigma_e^2} - \frac{(y - \Delta_y)^2}{2\sigma_\ell^2 f_R(x - \Delta_x)}\right]. \tag{A1}$$

Performing the y-integral gives

$$\epsilon(\Delta_x, \Delta_y) = \frac{I_\ell I_e}{2\pi\sigma_{ex}} \int \frac{dx}{\sigma_s(x, \Delta_x)}$$
$$\times \exp\left[-\frac{x^2}{2\sigma_{ex}^2} - \frac{\Delta_y^2}{2\sigma_s(x, \Delta_x)^2}\right], \tag{A2}$$

where

$$\sigma_s(x, \Delta_x) = \sqrt{\sigma_{ey}^2 + \sigma_\ell^2 f_R(x - \Delta_x)}. \tag{A3}$$

In the approximation of an infinite Rayleigh range the equations reduce to the more familiar form with [5]

$$\sigma_m = \sqrt{\sigma_e^2 + \sigma_\ell^2} \tag{A4}$$

and

$$\epsilon(\Delta_y) = \frac{1}{\sqrt{2\pi}\sigma_m} \exp-\frac{(\Delta_y)^2}{2\sigma_m^2}. \tag{A5}$$

Scans using the laser TM$_{01}$ *mode*

Using the same conventions as in Sec. III A 2, the light intensity of the laser TM$_{01}$ mode has the form

$$I_\ell(x, y, z) = \frac{I_0}{2\pi\sigma_\ell^2} \frac{1}{f_R(x)}\left(\frac{y^2}{\sigma_\ell^2 f_R(x)}\right)\exp\left[-\frac{y^2 + z^2}{2\sigma_\ell^2 f_R(x)}\right]. \tag{A6}$$

The necessary overlap integral is now

$$\epsilon(\Delta_x, \Delta_y) = \int \frac{dxdyI_\ell I_e}{(2\pi)^{3/2}\sigma_{ex}\sigma_{ey}\sigma_\ell\sqrt{f_R(x - \Delta_x)}}$$
$$\times \left(\frac{(y - \Delta_y)^2}{\sigma_\ell^2 f_R(x - \Delta_x)}\right)$$
$$\times \exp\left[-\frac{x^2}{2\sigma_{ex}^2} - \frac{y^2}{2\sigma_e^2} - \frac{(y - \Delta_y)^2}{2\sigma_\ell^2 f_R(x - \Delta_x)}\right], \tag{A7}$$

where, as before, Δ_x and Δ_y are the horizontal and vertical relative displacements of the electron and laser beams. Performing the y-integral gives

$$\epsilon(\Delta_x, \Delta_y) = \frac{I_\ell I_e}{2\pi\sigma_{ex}} \int \frac{dx}{\sigma_s(x, \Delta_x)}\left(\frac{\sigma_{ey}}{\sigma_s(x, \Delta_x)}\right)^2$$
$$\times \left[1 + f_R(x - \Delta_x)\left(\frac{\sigma_\ell\Delta_y}{\sigma_s(x, \Delta_x)}\right)^2\right]$$
$$\times \exp\left[-\frac{x^2}{2\sigma_{ex}^2} - \frac{\Delta_y^2}{2\sigma_s(x, \Delta_x)^2}\right], \tag{A8}$$

where $\sigma_s(x, \Delta_x)$ is as defined in Eq. (A3). For the TM$_{01}$ mode, the condition that 99% of the light energy is contained within the lens aperture becomes

$$0.99 = \int_0^{D_\ell/2} \int_0^{2\pi} rdrd\phi \frac{1}{2\pi\sigma_\ell^2}$$
$$\times \left(\frac{r}{\sigma_\ell}\right)^2 \sin^2\phi \exp\left[-\frac{r^2}{2\sigma_\ell^2}\right], \tag{A9}$$

which gives

$$0.01 = \left(1 + \frac{D_\ell^2}{8\sigma_\ell^2}\right)\exp\left[-\frac{D_\ell^2}{8\sigma_\ell^2}\right] \tag{A10}$$

and hence $D_\ell \simeq 1.15 \times 2\pi\sigma_\ell$. So for the TM$_{01}$ calculations performed in Sec. III A 3, a correction factor of 1.15 was applied, such that

$$\sigma_0|_{\text{TM}_{01}} = 1.15\lambda f_\#. \tag{A11}$$

[1] B. Barish *et al.*, http://www.linearcollider.org/wiki/doku.php?id=bcd:bcd_home, 2007.
[2] B. Barish *et al.*, http://www.linearcollider.org/cms/, 2007.
[3] R. Brinkmann *et al.*, DESY-01-011, 2001.
[4] M. Ross, in *Handbook of Accelerator Physics and Engineering*, edited by A. Chao and M. Tigner (World Scientific, Singapore, 1999), pp. 565–566.
[5] P. Tenenbaum and T. Shintake, Annu. Rev. Nucl. Part. Sci. **49**, 125 (1999).
[6] M. Minty and F. Zimmermann, *Measurement and Control of Charged Particle Beams* (Springer, Berlin, 2003).

I. AGAPOV, G. A. BLAIR, AND M. WOODLEY

Phys. Rev. ST Accel. Beams **10,** 112801 (2007)

[7] J. Seeman, in *Handbook of Accelerator Physics and Engineering*, edited by A. Chao and M. Tigner (World Scientific, Singapore, 1999), pp. 559–562.

[8] H. Wiedemann, *Particle Accelerator Physics I* (Springer, Berlin, 1999).

[9] P. Bryant, Proceedings of the CERN Accelerator School (CERN Report No. CERN-94-01, 1994), Vol. 1, p. 159.

[10] J. Rossbach and P. Schmuesser, Proceedings of the CERN Accelerator School (CERN Report No. CERN-94-01, 1994), Vol. 1, p. 17.

[11] K. L. Brown and R. Servranckx, AIP Conf. Proc. **127**, 62 (1985).

[12] P. Emma and M. Woodley, SLAC-PUB-8581, 1999.

[13] C. Golub and C. van Loan, *Matrix Computations*, Lecture Notes in Mathematics (The Johns Hopkins University Press, Baltimore, 1996), 3rd ed.

[14] W. Press, S. Teukolsky, W. Vetterling, and B. Flannery, *Numerical recipes in C + +* (Cambridge University Press, Cambridge, England, 2005), 2nd ed.

[15] The NLC design group, SLAC-R-0474, 1996.

[16] E. D. Courant and H. S. Snyder, Ann. Phys. (Leipzig) **3**, 1 (1958).

[17] T. Raubenheimer and R. D. Ruth, Nucl. Instrum. Methods Phys. Res., Sect. A **302**, 191 (1991).

[18] P. Eliasson and D. Schulte, EUROTEV-REPORT-2005-021, 2005.

[19] A. Seryi, L. Hendrickson, and G. White, contributed to the 36th ICFA Advanced Beam Dynamics Workshop (NANOBEAM 2005), Kyoto, Japan, 2005, 2006.

[20] S. T. Boogert *et al.*, UCRL-CONF-216283, www.llnl.gov/tid/lof/documents/pdf/326312.pdf, 2005.

[21] M. Woods *et al.*, contributed to the European Particle Accelerator Conference (EPAC 06), Edinburgh, Scotland, 2006, http://jacow.org/.

[22] A. Bosco *et al.*, EUROTEV-REPORT-2006-093, 2006.

[23] V. Balakin *et al.*, Phys. Rev. Lett. **74**, 2479 (1995).

[24] Y. Honda *et al.*, Nucl. Instrum. Methods Phys. Res., Sect. A **538**, 100 (2005).

[25] B. I. Grishanov *et al.*, arXiv:physics/0606194.

[26] M. Price *et al.*, prepared for European Particle Accelerator Conference (EPAC 06), Edinburgh, Scotland, 2006, http://jacow.org/.

[27] S. T. Boogert *et al.*, prepared for European Particle Accelerator Conference (EPAC 06), Edinburgh, Scotland, 2006, http://jacow.org/.

[28] C. Itzykson and J.-B. Zuber, *Quantum Field Theory* (McGraw-Hill, New York, 1980).

[29] A. E. Siegman, *Lasers* (University Science Books, Mill Valley, CA, 1986).

[30] Y. Honda, Proceedings of the Laser-wire Mini-Workshop, Oxford, http://ilcagenda.linearcollider.org/contributionDisplay.py?contribId=1&sessionId=(2006).

[31] S. Dixit *et al.*, EUROTEV-REPORT-2006-041, 2006.

[32] E. Bulyak and V. Skomorokhov, Phys. Rev. ST Accel. Beams **8**, 030703 (2005).